62p.

N62-16698

NASA TN D-1385

TECHNICAL NOTE

D-1385

PANEL FLUTTER TESTS ON

FULL-SCALE X-15 LOWER VERTICAL STABILIZER

AT MACH NUMBER OF 3.0

By Herman L. Bohon

Langley Research Center
Langley Station, Hampton, Va.

NATIONAL AERONAUTICS AND SPACE ADMINISTRATION

WASHINGTON

October 1962

NATIONAL AERONAUTICS AND SPACE ADMINISTRATION

TECHNICAL NOTE D-1385

PANEL FLUTTER TESTS ON FULL-SCALE X-15 LOWER VERTICAL STABILIZER AT MACH NUMBER OF 3.0

By Herman L. Bohon

SUMMARY

Panel flutter tests were conducted on two full-scale vertical stabilizers of the X-15 airplane at a Mach number of 3.0 in the Langley 9- by 6-foot thermal structures tunnel at dynamic pressures from 1,500 psf to 5,000 psf and stagnation temperatures from 300° F to 660° F. Flutter boundaries were obtained for four of the five distinct types of panels which make up the vertical sides of the stabilizers. The boundaries consisted of a flat-panel boundary and a thermally buckled-panel boundary. The flat-panel boundaries were characterized by a reduction in dynamic pressure with increasing skin temperature; whereas, after thermal buckling the trend was reversed. The minimum dynamic pressure for flutter occurred at the intersection of the flat-panel and buckled-panel boundaries and represented a large reduction in the dynamic pressure over the extrapolated, unstressed value. As a result of panel flutter, three of the five distinct types of panels were modified to provide the required flutter margin on the design flight dynamic pressure of the aircraft.

INTRODUCTION

During the design period of the X-15 airplane, and indeed prior to its first flight, little was known concerning flutter of long narrow panels. Theoretical predictions and available experimental information applied only to panels with length-width ratios less than 5. Certain skin areas on the vertical-tail surface of the X-15 had an unsupported length of 66 inches and a width of 6.25 inches. These long, narrow panels were suspected of being susceptible to flutter within the design flight envelope of the airplane. To explore the possibility of panel flutter, a single test was made on the full-scale lower vertical stabilizer in the Langley 9- by 6-foot thermal structures tunnel under aerodynamic heating conditions at a Mach number of 3.0 and at the minimum tunnel dynamic pressure (at that time) of 3,200 psf. This value of dynamic

pressure corresponded to a 30-percent margin above the maximum value anticipated in flight. During the test, flutter of the long, narrow panels occurred immediately; hence flutter points could not be established. Therefore, an experimental program was undertaken to establish a flutter boundary for these panels on the vertical stabilizer.

Two full-scale lower vertical stabilizers of the X-15 airplane were tested in the Langley 9- by 6-foot thermal structures tunnel at stagnation temperatures from 300° F to 660° F and at dynamic pressures ranging from 1,500 psf to 5,000 psf. (Installation of a diffuser after the aforementioned initial test permitted a minimum dynamic pressure of 1,500 psf.) After several tests, other panels on the stabilizers previously thought to be flutter free were found to flutter at dynamic pressures within the range expected in flight. The program was extended to permit definition of flutter boundaries of each type of panel found susceptible to flutter. As a result of the investigation, flutter data were obtained for unstiffened panels with length-width ratios of 4 and 10 and corrugation-stiffened panels with length-width ratios of 1.5 and 10. This paper discusses the conduct of the program and the flutter data obtained. The data are presented herein in tabular form and are also summarized in the form of flutter boundaries to indicate the effects of aerodynamic heating. In addition, modifications for the prevention of flutter of these panels are discussed.

SYMBOLS

D_x	flexural stiffness of orthotropic panel (direction perpendicular to corrugations)
D_{xy}	twisting stiffness of orthotropic panel
E	Young's modulus
f	frequency of flutter
h	aerodynamic heat-transfer coefficient
l	panel length (parallel to airflow)
M	Mach number
p	static pressure
p_b	static pressure in bay behind panel

Δp differential pressure on panel, $p_b - p$

q dynamic pressure

T temperature

T_t stagnation temperature

ΔT increase of panel skin temperature

t time

w panel width (perpendicular to airflow)

w_e width of equivalent isotropic panel

$\beta = \sqrt{M^2 - 1}$

μ Poisson's ratio

τ panel skin thickness

τ_e thickness of equivalent isotropic panel

DESCRIPTION OF STABILIZERS, PANELS, AND INSTRUMENTATION

The upper and lower vertical stabilizers of the X-15 airplane are similar in construction and each has two sections: one section is fixed to the fuselage and the other is movable. The all-movable portion of the lower stabilizer is jettisonable to facilitate landing. One design of the jettisonable portion is nonrecoverable (now out of production) and the other design has provisions for ejecting a parachute which permits recovery for later use. The nonrecoverable and recoverable all-movable portions of the lower vertical stabilizer are the models used in this investigation and are hereinafter simply referred to as stabilizers.

Both stabilizers are of rib and spar construction and have a wedge-shape airfoil and a trapezoidal planform with a leading-edge sweep angle of 30°. The stabilizers have a total wedge angle of 10° and are 108 inches in length, 20.5 inches in width at the trailing edge, and 25 inches in height. All components of the stabilizers are constructed from Inconel X. The internal structure consists of a main spar (the

primary load carrying member) located approximately one-third of the length from the leading edge (the pivot point of the all-movable stabilizer), a bulkhead at the trailing edge, and internal ribs in the longitudinal direction. The general configuration of the nonrecoverable stabilizer is shown in figure 1(a). The overall dimensions are common to both stabilizers. The exposed surface on either side is a 0.037-inch-thick sheet riveted to the leading edge and the main spar and a 0.030-inch-thick sheet between the main spar and the trailing-edge bulkhead. The skin is attached to the internal ribs which separate the interior into four bays. A view of the internal rib attachment is shown in figure 1(b). The ribs are seamwelded to corrugated angles which, in turn, are spotwelded to rib caps. The rib caps are riveted to the exposed skin to form four panels of both the forward portion and rear portion of the vertical sides. Details of the internal ribs are shown in section A-A of figure 1(a).

The main spar is constructed from 0.020-inch-thick corrugated sheets, oriented as shown in figure 1(a). The attaching arrangement of the corrugated sheets to the exposed skin on either side is similar to that shown in figure 1(b) for the internal ribs. The trailing-edge bulkhead, which consists of two corrugated sheets spotwelded together, was removed for this investigation and replaced with a heavy aluminum plate which had vents to each of the bays for control of bay pressures during testing. The triangular closure rib on top of the stabilizer is reinforced externally with three hat-shape stiffeners. (See fig. 1(a).) In addition, corrugated sheet (corrugation oriented perpendicular to the airflow) is spotwelded to the internal surface of the closure rib.

Nonrecoverable Stabilizer

Details of the nonrecoverable stabilizer are shown in figure 2; the individual side panels have been designated A1 to A8 to facilitate further discussion. The skin of bays 1 and 4 (panels A1, A5 and A4, A8) is reinforced with 0.008-inch-thick corrugations spotwelded to the skin and oriented perpendicular to the airflow. The corrugation details are shown in sections A-A and B-B. On the left side of the stabilizer, panels A7 and A8 have small vertical channel stiffeners riveted to the skin in the positions shown by the dotted lines. On the right side similar vertical channels are riveted to each of the panels rear of the main spar and, in addition, panels A6 and A7 have channels along the longitudinal center line. Panels A2 and A3 forward of the main spar were unstiffened on both the left and right sides. The pertinent dimensions of the panels are given in figure 2.

Recoverable Stabilizer

Details of the recoverable stabilizer are shown in figure 3; the designation B has been used to identify the panels of this stabilizer. The rearmost portion of bays 2 and 3 serves as a parachute compartment (panel B9). The parachute compartment panels are 18.3 inches long and 12.5 inches wide and are reinforced with 0.012-inch-thick corrugated sheet, the details of which are shown in sections A-A and B-B. Panel B5 had, in addition to the corrugation backing, small vertical channel stiffeners on both sides of the stabilizer riveted to the skin at the location shown in figure 3. Panels B6 and B7 on both sides of the stabilizer were stiffened with channels similar to those on the corresponding panels on the right side of the nonrecoverable stabilizer. All other details are the same as those shown in figure 2.

Panels

As already seen, the vertical sides of the two stabilizers consist of several panels of different length-width ratios and structural characteristics. However, as seen in figures 2 and 3, some of the panels are very similar in size and construction; therefore, for the purpose of this investigation and to simplify further discussion such panels are grouped as follows. Panels A2, A3, B2, and B3 are considered unstiffened panels with a length-width ratio of 4. Panels A6 and A7, on the left side, are unstiffened panels with a length-width ratio of 10. Panels A1 and B1 are corrugation-stiffened panels with a length-width ratio of 4; panels A5 and B5 are corrugation-stiffened panels with a length-width ratio of 10. Panel B9 is a corrugation-stiffened panel with a length-width ratio of 1.5.

Panel A7 on the left side of the nonrecoverable stabilizer had a small lateral channel stiffener (fig. 2); however, no attempt was made to isolate the behavior of this panel from the adjacent panel A6. Consequently, panel A7 on the left side was grouped with panel A6 as an unstiffened panel with a length-width ratio of 10 and, likewise, both panels B5 and panel A5 on the right side were considered corrugation-stiffened panels with a length-width ratio of 10. However, panels A6 and A7 on the right side, as well as all panels B6 and B7, were reinforced with both lateral and longitudinal stiffeners which were intended to prevent panel flutter within the dynamic-pressure range of the aircraft. These stiffeners are discussed in detail in the section entitled "Panel Stiffeners." Panels A4, A8, B4, and B8 were immobilized by the mounting arrangement and, consequently, are not considered in this investigation. Thus, five distinct types of panels are considered: unstiffened panels with length-width ratios of 4 (panels A2, A3, B2, and B3) and 10 (panels A6 and A7), and corrugation-stiffened panels with length-width ratios of 1.5 (panel B9), 4 (panels A1 and B1), and 10

(panels A5 and B5). The geometric properties of each of these panels are summarized in table I.

Also listed in table I are remarks on structural alteration or instrumentation changes made to certain panels during the investigation. These changes are discussed in detail in subsequent sections.

Instrumentation

Each stabilizer was instrumented with iron-constantan thermocouples to measure skin temperatures during tests. Inductance-type deflectometers were used to determine the panel behavior by measuring the change in inductance as a function of the distance between the deflectometer and the skin. The deflectometers were located approximately one-quarter inch behind the panel skin. In addition, strain gages were attached to some panel skins to corroborate the deflectometer data. Quick-response, strain-gage-type pressure transducers were used to measure the static pressure along the external surface of the stabilizers and the pressures in bays 2 and 3, both forward and rear of the main spar. High-speed 16-mm motion pictures supplied supplementary data on panel behavior. The exterior surface was painted to form grid lines for photographic purposes.

The locations of the instrumentation are shown in figure 4 for the nonrecoverable stabilizer and in figure 5 for the recoverable stabilizer. The instrumentation shown represents that available during the latter part of the investigation. All changes in instrumentation during the investigation are summarized in table I. All data were recorded on either oscillographs or magnetic tapes.

TEST APPARATUS AND PROCEDURE

Test Facility

All tests were conducted in the Langley 9- by 6-foot thermal structures tunnel, an intermittent blowdown facility operating at a Mach number of 3.0 and exhausting to the atmosphere. This tunnel is currently capable of producing dynamic pressures from 1,400 psf to 5,000 psf and stagnation temperatures from 200° F to 660° F. A detailed description of the operating characteristics is given in reference 1.

Test Procedure

Preparatory to testing, a stabilizer was mounted on the floor of the test section in an inverted position and bolted at the main spar. Heavy angle shoes were fixed to the tunnel floor along each side of the stabilizer at the base to prevent horizontal motion. In some tests these shoes extended along the entire length of the stabilizer, whereas for other tests only the downstream half of the stabilizer was restrained by the shoes. The latter arrangement is shown in figure 6.

During tunnel start and shutdown, severe turbulence resulting from flow separation from the tunnel walls imposed abnormal loads on the stabilizers. In addition, the sudden drop in test-section static pressure during tunnel start necessitated a rapid drop of the bay pressures. This bay-pressure drop was accomplished by mounting a heavy box, having the contour of the stabilizer (fig. 6), at the trailing edge with a small slot between the box and stabilizer, to which each bay was vented. During a test the detached box also served to maintain a pressure in the stabilizer bays of essentially free-stream static pressure so that the differential pressure across the panels was near zero. In addition, the detached box prevented pressure from feeding upstream through the subsonic wake from the normal shock wave located just downstream from the test section at the minimum dynamic pressure. Also shown in figure 6 are the access doors in the length-width-ratio-4 panels (panels A2 and A3), which were necessary for installation of instrumentation on the opposite panels.

Tests were conducted at a Mach number of 3.0 and at stagnation pressures from 1,500 psf to 5,000 psf. For all but one test the stagnation temperature was held at a preset value which varied for different tests from 300° F to 660° F. For the one test, however, the stagnation temperature was increased gradually from 230° F to 370° F. This change in stagnation temperature (though not a normal test condition) was accomplished by cooling the forward portion of the heat exchanger. For most tests the dynamic pressure at tunnel start was less than 2,500 psf to keep the initial loads at a minimum and was varied thereafter.

For four tests on the nonrecoverable stabilizer, heavy longitudinal stiffeners were fixed to the exposed surface of the unstiffened panels with a length-width ratio of 10 (panels A6, A7). (See table I.) This procedure permitted further testing at higher dynamic pressures without possible failure of these weaker panels due to flutter and effectively immobilized these panels so that their motion could not influence the flutter of adjacent panel A5.

RESULTS AND DISCUSSION

Seven tests were made on the nonrecoverable stabilizer and eight on the recoverable stabilizer. In 13 of the 15 tests, flutter was induced in at least one of the five distinct types of panels which make up the vertical sides of the stabilizers. Panels found susceptible to flutter within the dynamic-pressure range considered in this investigation were the unstiffened panels with length-width ratios of 4 (panels A2, A3, B2, and B3) and 10 (panels A6 and A7) and the corrugation-stiffened panels with length-width ratios of 1.5 (panel B9) and 10 (panels A5 and B5). The corrugation-stiffened panels with a length-width ratio of 4 (panels A1 and B1) did not flutter during this investigation. In 11 tests the dynamic pressure was maintained constant during the first portion of the tests so that flutter of the initially flat panels was caused entirely by thermal stresses induced by aerodynamic heating; for other tests the dynamic pressure was increasing when flutter started. In 12 tests the flutter stopped, after which the panels were observed to be in a stable, buckled condition.

Basic data are presented in figures 7 to 13 for the nonrecoverable stabilizer and in figures 14 to 21 for the recoverable stabilizer; test and panel conditions when flutter started and stopped are summarized in tables II and III. In the figures, part (a) shows the differential pressure on the designated panel - positive when the bay pressure exceeds the panel static pressure; part (b) shows the variation of the tunnel dynamic pressure during the tests; and part (c) presents the tunnel stagnation temperature and panel skin temperatures. All tunnel and model conditions are plotted as a function of time. Table II gives the results at the start and termination of flutter for the unstiffened panels (length-width ratios of 4 and 10) and table III gives the results for the corrugation-stiffened panels (length-width ratios of 1.5 and 10). The results for the unstiffened panels with a length-width ratio of 10 (table II) have also been presented in reference 2 in which the effect of panel material and size on flutter of aerodynamically heated panels is shown. These data are repeated herein to permit complete representation of flutter data on the vertical stabilizer of the X-15 airplane. The data tabulated for the start and termination of flutter are the time t, flutter frequency f, dynamic pressure q, panel differential pressure Δp, incremental skin temperature ΔT, and the thickness-ratio parameter given by theory $\left(\frac{\beta E}{q}\right)^{1/3}\frac{\tau}{l}$. For tests for which no data are shown under "End of flutter," either the panels continued to flutter until the end of the test or data were incomplete because of instrumentation failure.

Differential Pressures

As was mentioned in the section entitled "Test Procedure," the test-section static pressure dropped rapidly (approximately 10 psi in 1 second) during tunnel start and imposed large transient loads on the panels unless followed closely by a decrease in bay pressure. The technique used to control the bay pressures to the rear of the main spar was adequate in that differential pressures on these panels were generally less than 0.5 psi during tunnel start. The bays forward of the main spar, however, were not vented to the airstream as were the rear bays, and pressure was permitted to escape only through small openings (provided for instrumentation leads) in the main spar and around the supports. Thus, the pressure of the forward bays lagged the panel static pressures approximately two-tenths of a second during tunnel start, which was sufficient to cause temporary differential pressures exceeding 2 psi on the panels. These results are plotted in figures 10(a), 11(a), and 12(a) for the nonrecoverable stabilizer and, similarly, in figures 18(a), 19(a), and 20(a) for the recoverable stabilizer.

The static-pressure gage on the corrugation-stiffened panel with a length-width ratio of 1.5 (panel B9) did not function properly for tests 8 to 11; therefore, for these tests the panel static pressure was determined by multiplying the ratio of panel static pressure to free-stream stagnation pressure for test 14 by the appropriate test stagnation pressures. The differential pressures shown in figures 14(a) to 17(a) were obtained in this manner.

Panel Temperatures

The stabilizer skin was not protected from aerodynamic heating during tunnel start and, consequently, for the approximately 1.5 seconds required to establish constant-flow conditions, skin temperature increases were sufficiently great, in a few instances, to initiate flutter. However, supersonic flow was established as early as 0.7 second and, although test conditions varied rapidly between 0.7 and 1.5 seconds, the flow was uniform. In each test where flutter-start data were obtained during this time interval, observation of deflectometer records and/or high-speed motion pictures indicated that panel disturbance from the tunnel start shock wave had ceased and the panel was motionless just prior to the onset of flutter. Therefore, data obtained during this time interval are considered valid. The accuracy of measured temperatures and pressures chosen for the start of flutter under these highly transient conditions is probably less than the accuracy obtained during constant-flow conditions.

For the first few tests on each stabilizer thermocouple and deflectometer data were not obtained on the unstiffened panels forward of the

main spar (table I); however, for the recoverable stabilizer, high-speed motion pictures were available to study the behavior of these panels. For such tests in which flutter was observed, skin temperatures were calculated according to the following procedure. Experimental values of the aerodynamic heat-transfer coefficient h were derived from the available temperature histories (figs. 18(c), 19(c), 20(c), and 21(c)) by the procedure used in reference 3. These values were then compared with theoretical values of h obtained by the method of reference 4, wherein local flow conditions dictated by the stabilizer wedge angle were used. The average experimental value of h was 15 percent less than that calculated. Reducing the theoretical value of h by 15 percent made the calculated temperature histories consistent with the available experimental temperature histories. This adjustment was then applied to theoretical values of h for tests wherein calculated temperatures were required. The equilibrium temperature used in the calculations was obtained by using local flow conditions and assuming a turbulent recovery factor. The temperature histories shown in figures 14(c), 15(c), 16(c), and 17(c) by the dashed line were calculated in this manner.

In addition to the forward panels, temperature histories were also lacking for the corrugation-stiffened panels with a length-width ratio of 10 (panels A5 and B5); in fact, only one test (test 15, panel B5) was made from which skin temperatures were obtained on these panels. The results of this one test do not permit adequate comparison of experimental and theoretical heat-transfer coefficients for calculating temperatures by using the method just described for the panels forward of the main spar. In addition, local flow conditions in the vicinity of panel B5 were not as well defined as were the flow conditions for the panels forward of the main spar. However, in order to show a flutter trend for the corrugated panel, skin temperatures for the recoverable-stabilizer panel (panel B5) were estimated by using the temperature histories of the length-width-ratio-1.5 panel (panel B9) as a guide. The ratio of the temperature of thermocouple 10 to the average temperature of thermocouples 6 and 8 (fig. 21(c)) was plotted as a function of time for test 15 and the ratio, for a given time, was assumed to remain constant for other values of the dynamic pressure and stagnation temperature. Then, for each test the temperature of the corrugation-stiffened panel with a length-width ratio of 10 corresponding to the time recorded for the start and stop of flutter was estimated by multiplying the appropriate ratio by the measured temperature of the length-width-ratio-1.5 panel. This procedure, though purely arbitrary, corrects somewhat for the different heating rates which result from change in the dynamic pressure and/or stagnation temperature for the various tests. Any error introduced by this procedure would at least be systematic so as not to affect seriously the overall flutter trend. The differential temperatures for panel B5 shown in table III for tests 9, 11, and 14 were obtained in this manner. No attempt was made to estimate

the temperatures for the start and stop of flutter for the corresponding panel (A5) on the nonrecoverable stabilizer since no temperature histories were available to use as a basis of comparison.

Unstiffened-Panel Flutter Results

The overall effect of aerodynamic heating on flutter of the unstiffened panels with length-width ratios of 4 and 10 is shown in figure 22, where values of the thickness-ratio parameter $\left(\frac{\beta E}{q}\right)^{1/3}\frac{\tau}{l}$ are plotted as a function of the incremental skin temperature ΔT. The open symbols represent flutter-start points where the panels were flat prior to the start of flutter; the solid symbols represent flutter-stop points where the panels were buckled upon cessation of flutter. The open symbol with a tick mark (fig. 22(a)) indicates a flutter-stop point for which the panel appeared to be in a flat, stable condition at the end of flutter. This test is indicated by the notation a in table II. The lines faired through the flutter points, then, are the boundaries separating the flutter region from the stable region.

As can be seen from figure 22, the flutter boundaries consist of a flat-panel boundary, a buckled-panel boundary, and a transition region at the intersection of the flat-panel and buckled-panel boundaries. The flat-panel boundary shows that, as the skin temperature increases, the dynamic pressure must decrease if flutter is to be prevented. At transition, the trend is reversed and the buckled-panel boundary shows that an increase in skin temperature requires an increase in the dynamic pressure for flutter to occur. The characteristics of these boundaries are very similar to those shown in reference 1. In this reference the buckled boundary was defined by flutter-start points where the panels (just prior to flutter) were in a buckled but stable state, as well as by flutter-stop points described herein. Therefore, the transition point defines the maximum value of the thickness-ratio parameter, or minimum value of the dynamic pressure, for which flutter will occur. For the panels with length-width ratios of 4 and 10, the values of the dynamic pressure at the extrapolated, unstressed points (intersection of the flat-panel boundary and the ordinate) are approximately 2,460 psf and 1,930 psf, respectively, which are less than the design supersonic dynamic pressure (2,500 psf) of the aircraft. In addition, with aerodynamic heating present, the flutter boundaries at the transition points show a reduction in dynamic pressure of about 36 percent as compared with the extrapolated, unstressed values of dynamic pressure for each panel and, consequently, both panels appear to be highly susceptible to flutter within the flight envelope. The transition points occurred at skin-temperature increases of 50° F and 60° F for the panels with length-width ratios of 10 and 4, respectively.

Application of these data to actual flight conditions would require a detailed analysis of the panel buckling characteristics. Since the panel buckling characteristics are dependent on the supporting-structure temperature as well as the panel temperature, the transition from the flat- to buckled-panel boundaries could occur, in flight, at temperatures other than those shown in figure 22. However, the maximum values of the thickness-ratio parameter are not expected to be affected.

Of the six tests listed in table II for the length-width-ratio-4 panels, the time of flutter for four of these was determined from high-speed motion pictures since no other instrumentation was provided for these first few tests. After installation of the instrumentation, only two tests (test 5 on the nonrecoverable stabilizer and test 15 on the recoverable stabilizer) were made for which flutter was ascertained. For three other tests not listed in table II (tests 6, 12, and 14) tunnel conditions were such (figs. 12, 18, and 20) that these panels should have fluttered, based on the faired boundary of figure 22(a). In tests 6 and 14, however, the deflectometers did not function properly and, although some motion was observed from the motion pictures, camera coverage was inadequate for positive definition of flutter. For test 12, the dynamic pressure was sufficiently high to place the panel well into the flutter region shown in figure 22(a); however, no flutter was evidenced from either the deflectometer records or motion pictures. It is not understood why flutter did not occur during this test. Nevertheless, the flutter points obtained from tests 5 and 15 agree with those from the other four tests and confirm the position of the flutter boundary.

Corrugation-Stiffened-Panel Flutter Results

Effective panel geometry.- Listed in table III are the effective length-width ratios and effective skin thicknesses for the corrugated panels. The effective panel widths and thicknesses were calculated by the method presented in reference 5. In this reference the geometric and elastic properties of an orthotropic panel are used to determine geometric properties of an equivalent isotropic panel in order to permit comparison of orthotropic panel flutter results with isotropic panel theory. For aerodynamic purposes the panel length is unchanged and the effective width and thickness are determined from the following equations:

$$w_e = w\left(\frac{D_x}{D_{xy}}\right)^{1/2}$$

$$\tau_e = \left[12\left(1 - \mu^2\right)\frac{D_x}{E}\right]^{1/3}$$

where w is the actual panel width and D_x and D_{xy} represent the orthotropic panel flexural and twisting stiffnesses, respectively. The procedure used to calculate the stiffnesses D_x (stiffness in direction of airflow and perpendicular to direction of corrugations) and D_{xy} is presented in reference 6.

Effect of aerodynamic heating on flutter.- Flutter boundaries for the corrugation-stiffened panels with length-width ratios of 1.5 and 10 are presented in figure 23 where values of the thickness-ratio parameter obtained from table III are plotted as a function of the incremental skin temperature. As before, the open symbols represent flutter-start points where the panels were flat prior to the start of flutter, and the solid symbols represent flutter-stop points where the panels were stable but buckled upon cessation of flutter.

Although data are limited, the boundaries represent the first flutter data available on corrugation-stiffened panels where aerodynamic heating is encountered. As seen in figure 23, the flutter characteristics are similar to those of the unstiffened panels; however, the apparent magnitudes of the effects of aerodynamic heating differ from those for the unstiffened panels. At the extrapolated, unstressed points, the values of the dynamic pressure (5,700 psf and 5,800 psf for the panels with length-width ratios of 1.5 and 10, respectively) are considerably greater than the design dynamic pressure of the aircraft; however, for each panel aerodynamic heating effectively reduced the dynamic pressure for flutter (at the transition point) by 58 percent of the extrapolated values. Consequently, both panels would have less than a 30-percent flutter margin within the design flight envelope where aerodynamic heating is encountered.

The incremental temperatures at the transition points are approximately 110° F and 150° F for the panels with length-width ratios of 10 and 1.5, respectively. Again, values of the incremental temperature at the transition points (fig. 23) are not directly applicable to flight conditions without detailed knowledge of the temperature history of the internal structure and the resulting panel buckling characteristics. For these corrugation-stiffened panels the temperature gradient through the corrugations (for example, fig. 21(c)) presents an additional factor. The temperature gradient existing in the wind-tunnel tests may cause considerable spanwise curvature tending to stiffen the panel against flutter. In flight, a much lower heating rate would be expected and temperature variation through the corrugations may be negligible.

Consequently, in flight, values of the thickness-ratio parameter for flutter may also differ from those values shown in figure 23.

Of the tests on the length-width-ratio-10 panel (panel B5) for which flutter-start points were obtained, the first two tests (tests 9 and 11, table III) resulted in values of the incremental skin temperature at flutter which were nearly twice the corresponding values indicated by the faired boundary in figure 23(b). These two points are indicated by the square symbols in figure 23(b). However, close inspection of the stabilizer during the investigation revealed progressive deterioration of spot-welds between the corrugation and exposed skin along several of the corrugations at the rearmost portion of the panel. Although this failure appeared insignificant in view of the overall length of the panel, other possible interior deterioration not accessible to visual inspection could decrease the panel stiffness considerably and account for the discrepancy in the results. In view of this, the minimum dynamic pressure for flutter of the initial (undamaged) panel may be more closely approximated by a boundary faired through the square symbols which would intersect the existing buckled-panel boundary at approximately 2,900 psf.

A comparison of the dynamic pressures at flutter of the length-width-ratio-10 panels (panels A5 and B5) on the nonrecoverable and recoverable stabilizers given in table III indicates that the panel on the nonrecoverable stabilizer fluttered at a much lower dynamic pressure than did the corresponding panel on the recoverable stabilizer. As seen in figures 2 and 3, the panels on the two stabilizers differ slightly in construction by the omission of the lateral stiffener on the left side of the nonrecoverable stabilizer; thus, some difference in their flutter behavior may be expected. Although panel A5 on the right side of the stabilizer had a lateral stiffener (fig. 2), the flutter characteristics of this panel appeared to be the same as those of the panel on the left side. Such behavior, however, may have been due to motion transmitted through the internal ribs during flutter of the left side. For this condition the data in table III for panel A5 would apply only to the panel without the lateral stiffener. For each test listed in table III wherein flutter of panel A5 occurred, the adjacent panel A6 was reinforced externally with longitudinal channels (table I) so as not to influence the behavior of panel A5. Unfortunately, the lack of temperature data for panel A5 prohibits comparison of its flutter boundary with that of panel B5 shown in figure 23(b).

Panel Stiffeners

Three of the five distinct types of panels on the X-15 stabilizer were modified to provide an adequate flutter margin. Those modified were the unstiffened panels with length-width ratios of 4 and 10 and the

corrugation-stiffened panel with a length-width ratio of 1.5. The corrugation-stiffened panel with a length-width ratio of 10 appeared to be marginal but was believed to be sufficiently safe from flutter in actual flight. The panels with length-width ratios of 4 and 10 were stiffened with 0.030-inch-thick by 15/16-inch-deep Inconel X channels riveted along the lateral and longitudinal center lines. As noted in the section entitled "Panels," the length-width-ratio-10 panels A6 and A7 on the right side of the nonrecoverable stabilizer as well as all panels B6 and B7 on the recoverable stabilizer were reinforced with these stiffeners, and throughout this investigation these stiffeners proved to be adequate for the prevention of flutter. The length-width-ratio-1.5 panel B9 was reinforced with a 0.012-inch-thick hat-shape stiffener riveted along the longitudinal center line. The dimensions and locations of these stiffeners are shown in figure 24. The stiffeners were installed on the length-width-ratio-4 panel of the nonrecoverable stabilizer and on the length-width-ratio-1.5 corrugation-stiffened panel of the recoverable stabilizer, and final tests (tests 7 and 15) were conducted at a dynamic pressure of 3,200 psf without evidence of flutter. These stiffeners are now incorporated in the production model of the X-15 stabilizer.

Comparison of Flutter Results With Envelope Curve

The flutter results of this investigation are compared with the experimental envelope reproduced from reference 5 in figure 25. The envelope is a plot of the thickness-ratio parameter as a function of the length-width ratio, where τ_e and w_e are either actual dimensions for isotropic panels or effective dimensions for orthotropic panels. The curve represents a boundary faired through maximum values of the thickness-ratio parameter for all available experimental panel flutter data (at that time) of both isotropic and orthotropic panels. The panel flutter results obtained during the present investigation are indicated by the bars at the actual length-width ratios for the isotropic panels and the effective length-width ratios for the corrugated panels. The lengths of the bars represent the effect of aerodynamic heating as shown in figures 22 and 23.

As can be seen in figure 25, the comparison is not good; only the data for the corrugation-stiffened length-width-ratio-10 panel ($l/w_e = 69.70$) match the curve. For the unstiffened panels with length-width-ratios of 10 and 4 the envelope curve is, respectively, conservative and unconservative. The envelope curve was determined from data of panels at zero angle of attack. However, when the effect of the stabilizer wedge angle on the Mach number and dynamic pressure is considered, the maximum value of the thickness-ratio parameter for the length-width-ratio-4 panels would be reduced only from 0.265 to 0.24; this reduction,

based on the envelope curve, still implies that a rather large reduction in skin thickness would be permissible before flutter would occur. Nevertheless, as shown in reference 2 the value of the thickness-ratio parameter at the transition point for a given panel is directly related to the stress ratio and, therefore, may differ considerably with changes in supporting structure. This factor and other factors which affect the flutter characteristics of a panel cannot be accounted for by a simple plot such as shown in figure 25. Consequently, if the envelope curve is used as a basis of design, such discrepancies as indicated by these data must be expected.

The flutter data for the length-width-ratio-1.5 panel ($l/w_e = 11.67$) are well within the indicated no-flutter region of the envelope curve. However, it was implied in reference 5 that the simplified analysis presented for comparing orthotropic panels with isotropic panels may not be adequate for low effective length-width ratios. The results from tests of the length-width-ratio-1.5 panel also indicate that a more thorough analysis may be necessary.

CONCLUDING REMARKS

Two full-scale lower vertical stabilizers of the X-15 airplane were tested in the Langley 9- by 6-foot thermal structures tunnel to determine the flutter characteristics of the vertical side panels under aerodynamic heating conditions and to proof test modifications necessary for the prevention of panel flutter within the proposed flight envelope of the aircraft. Tests were conducted at a Mach number of 3.0 and stagnation temperatures between 300° F and 660° F for a range of dynamic pressure from 1,500 psf to 5,000 psf.

Four distinct types of surface skin panels were found to have less than a 30-percent flutter margin on the design supersonic flight dynamic pressure of 2,500 psf. Two panels had length-width ratios of 4 and 10 and were unstiffened, and the other two panels had length-width ratios of 1.5 and 10 and had an internal corrugated sheet stiffener with corrugations oriented normal to the flow direction. Flutter boundaries for all panels showed similar trends and consisted of a flat-panel boundary, a thermally buckled-panel boundary, and a transition region at the intersection of the two boundaries. The transition point represented the minimum dynamic pressure for which flutter would occur under aerodynamic heating conditions. The dynamic pressure at the transition points represented a reduction over the extrapolated, unstressed value of approximately 36 percent for the unstiffened panels and 58 percent for the corrugation-stiffened panels.

The unstiffened panels with length-width ratios of 4 and 10 and the corrugation-stiffened panel with a length-width ratio of 1.5 were modified by attaching small stiffeners (now incorporated in the design) to the panel skins, and final tests assured the required flutter margin. A comparison of the flutter boundaries with the experimental envelope curve of NASA Technical Note D-451 indicated that for at least some length-width ratios the envelope curve is inadequate for predicting the minimum dynamic pressure for flutter.

Langley Research Center,
National Aeronautics and Space Administration,
Langley Station, Hampton, Va., June 4, 1962.

REFERENCES

1. Dixon, Sidney C., Griffith, George E., and Bohon, Herman L.: Experimental Investigation at Mach Number 3.0 of the Effects of Thermal Stress and Buckling on the Flutter of Four-Bay Aluminum Alloy Panels With Length-Width Ratios of 10. NASA TN D-921, 1961.

2. Guy, Lawrence D., and Bohon, Herman L.: Flutter of Aerodynamically Heated Aluminum-Alloy and Stainless-Steel Panels With Length-Width Ratio of 10 at Mach Number of 3.0. NASA TN D-1353, 1962.

3. Heldenfels, Richard R., Rosecrans, Richard, and Griffith, George E.: Test of an Aerodynamically Heated Multiweb Wing Structure (MW-1) in a Free Jet at Mach Number 2. NACA RM L53E27, 1953.

4. Lee, Dorothy B., and Faget, Maxime A.: Charts Adapted From Van Driest's Turbulent Flat-Plate Theory for Determining Values of Turbulent Aerodynamic Friction and Heat-Transfer Coefficients. NACA TN 3811, 1956.

5. Kordes, Eldon E., Tuovila, Weimer J., and Guy, Lawrence D.: Flutter Research on Skin Panels. NASA TN D-451, 1960.

6. Stroud, William Jefferson: The Bending and Twisting Stiffnesses of Corrugation Stiffened Panels. M. S. Thesis, Virginia Polytechnic Inst., 1962.

TABLE I.- SUMMARY OF GEOMETRIC PROPERTIES AND PANEL CONDITIONS

Panel	l/w	l, in.	τ, in.	Test	Remarks
Unstiffened panels					
A2, A3	4	27	0.037	1 to 3	No instrumentation.
				4 to 6	Access doors installed in left side. Panels instrumented as shown in figure 4.
				7	Panels stiffened with lateral and longitudinal channels.
B2, B3	4	27	.037	8 to 11	No instrumentation. Camera coverage only.
				12 to 15	Access doors installed in left side. Panels instrumented as shown in figure 5.
A6, A7	10	66	0.030	3	Panels on left side immobilized by channels bonded to exposed surface along longitudinal center line.
				4	External channels removed.
				5 to 7	Panels on left side immobilized by channels riveted to exposed surface along longitudinal center line.
Corrugation-stiffened panels					
B9	1.5	18.3	0.030	15	Both sides stiffened with hat section along longitudinal center line.
A1					
B1	4	27	0.037		
A5	10	62	0.030	3, 5 to 7	Adjacent panel A6 immobilized.
B5	10	62	.030	15	Thermocouples 9 and 10 added (fig. 5).

TABLE II.- SUMMARY OF FLUTTER CONDITIONS FOR UNSTIFFENED PANELS

$\left[E = 30.7 \times 10^6 \text{ psi}\right]$

Test	Panel	l/w	τ, in.	T_t, °F	Start of flutter						End of flutter				
					t, sec	f, cps	q, psf	Δp, psi	ΔT, °F	$\left(\frac{\beta E}{q}\right)^{1/3} \frac{\tau}{l}$	t, sec	q, psf	Δp, psi	ΔT, °F	$\left(\frac{\beta E}{q}\right)^{1/3} \frac{\tau}{l}$
5	A2, A3	4	0.037	500	1.25	---	2,200	-0.44	16	0.243	[a]2.25	1,835	-0.59	38	0.259
8	B2, B3	4	.037	310	4.10	---	1,800	-----	26	.259	21.20	1,900	-----	120	.254
9	B2, B3	4	.037	450	3.70	---	1,900	-----	47	.254	-----	-----	-----	---	-----
10	B2, B3	4	.037	230 to 370	3.70	---	3,180	-----	26	.215	22.23	2,200	-----	177	.243
11	B2, B3	4	.037	450	1.50	---	2,630	-----	17	.229	22.90	2,040	-----	256	.249
15	B2, B3	4	.037	640	----	260	-----	-----	--	-----	12.40	3,260	-----	310	.213
1	A6, A7	10	.030	436	2.20	250	1,560	.19	30	.091	18.60	1,730	-.11	180	.088
2	A6, A7	10	.030	440	.90	220	1,760	.03	10	.088	32.50	1,670	-.05	234	.089
4	A6, A7	10	.030	450	1.15	480	1,730	.32	19	.088	4.81	1,500	.20	66	.092

[a]Panel flat when flutter stopped.

TABLE III.- SUMMARY OF FLUTTER CONDITIONS FOR CORRUGATION-STIFFENED PANELS

$\left[E = 30.7 \times 10^6 \text{ psi}\right]$

Test	Panel	l/w	l/w_e	τ_e, in.	T_t, °F	Start of flutter						End of flutter				
						t, sec	f, cps	q, psf	Δp, psi	ΔT, °F	$\left(\frac{\beta E}{q}\right)^{1/3} \frac{\tau_e}{l}$	t, sec	q, psf	Δp, psi	ΔT, °F	$\left(\frac{\beta E}{q}\right)^{1/3} \frac{\tau_e}{l}$
9	B9	1.5	11.67	0.0305	450	10.00	200	3,060	[a]-0.70	101	0.270	22.05	2,600	[a]-0.30	195	0.285
10	B9	1.5	11.67	.0305	230 to 370	7.00	200	4,200	[a]-.55	40	.238	[b]21.90	2,600	[a]-.27	126	.285
11	B9	1.5	11.67	.0305	450	14.91	200	2,900	[a]-.65	143	.274	21.78	3,180	[a]-.42	186	.266
14	B9	1.5	11.67	.0305	500	7.71	170	2,850	.23	127	.274	13.30	2,850	.22	188	.274
3	A5	10	69.70	.0300	310	7.00	250	2,450	------	---	.0827	------	-----	------	---	------
5	A5	10	69.70	.0300	500	5.40	225	1,780	------	---	.0920	13.95	1,780	------	---	.0920
6	A5	10	69.70	.0300	500	3.60	220	2,220	------	---	.0859	7.45	2,220	------	---	.0859
7	A5	10	69.70	.0300	500	2.60	220	3,280	------	---	.0755	7.70	3,260	------	---	.0755
9	B5	10	69.70	.0300	450	13.00	300	3,780	------	107	.0718	------	-----	------	---	------
11	B5	10	69.70	.0300	450	20.00	---	3,460	------	151	.0740	------	-----	------	---	------
[c]14	B5	10	69.70	.0300	520	7.60	300	2,840	------	92	.0785	11.30	2,840	------	136	.0785
15	B5	10	69.70	.0300	640	4.10	240	3,260	------	72	.0755	23.10	3,260	------	300	.0755

[a]Differential pressure estimated.

[b]Panel flat when flutter stopped.

[c]Panel deterioration noted. (See section entitled "Corrugation-Stiffened-Panel Flutter Results.")

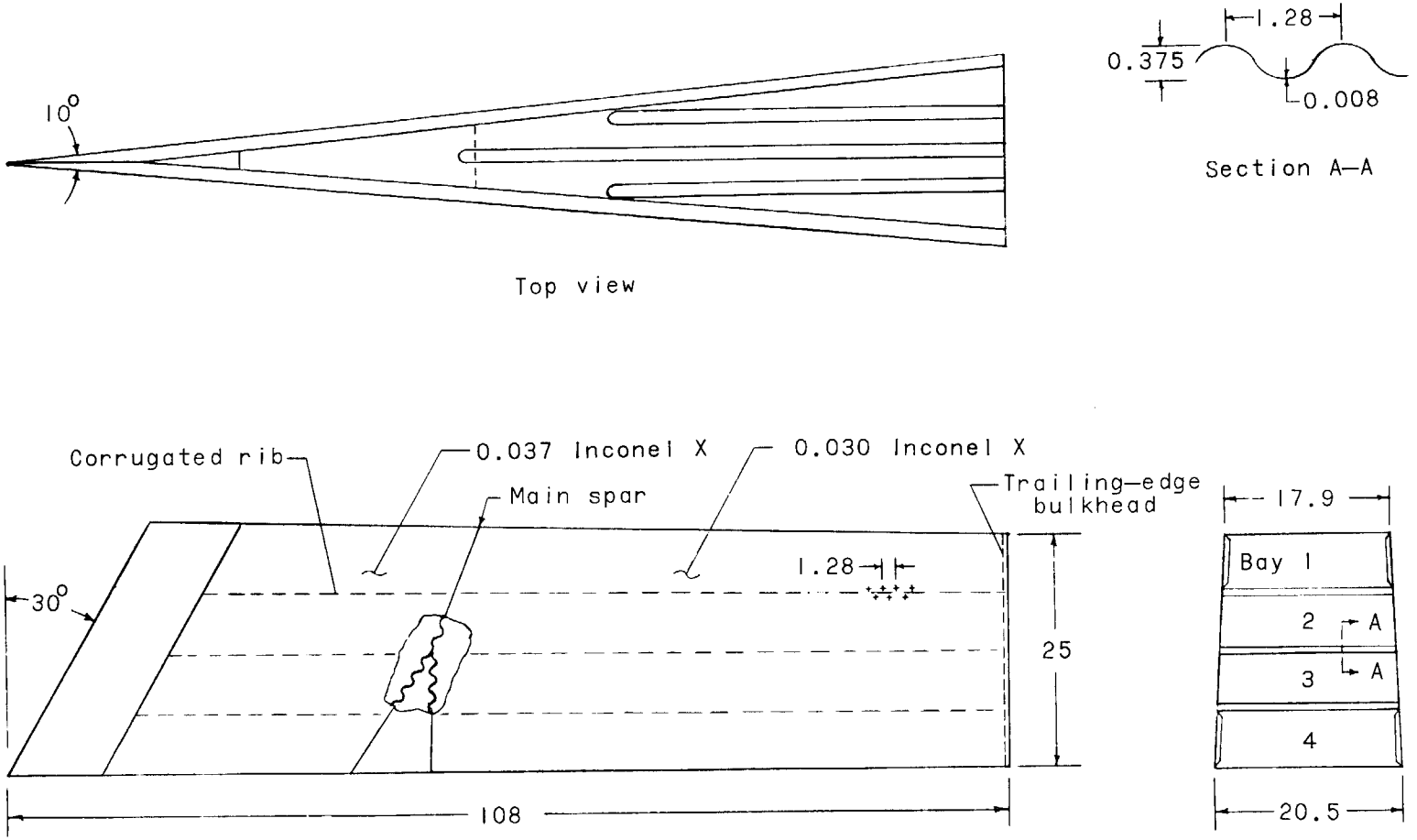

(a) General configuration.

Figure 1.- Lower vertical (nonrecoverable) stabilizer. All dimensions are in inches unless otherwise indicated.

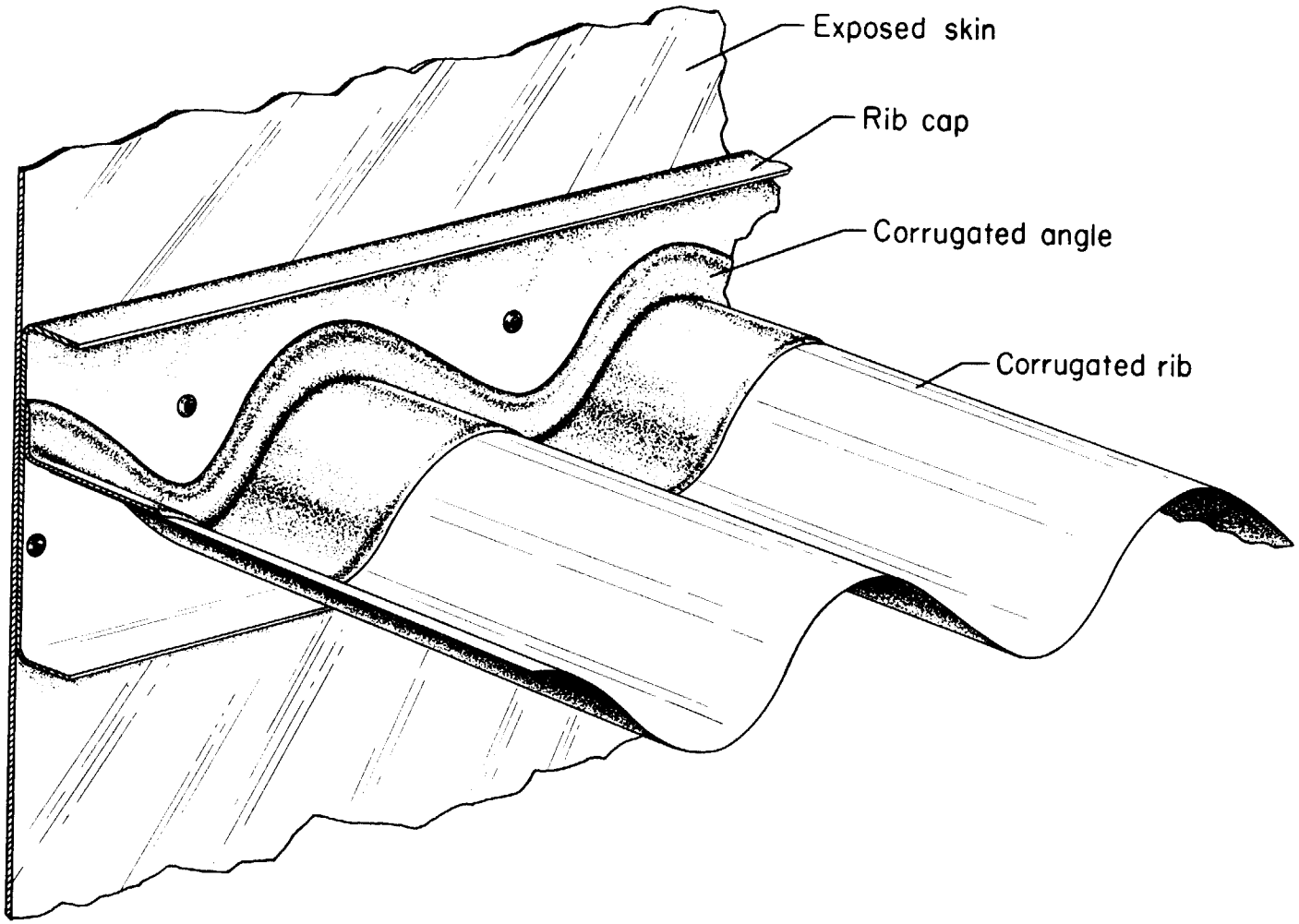

(b) View of skin and internal rib attachment.

Figure 1.- Concluded.

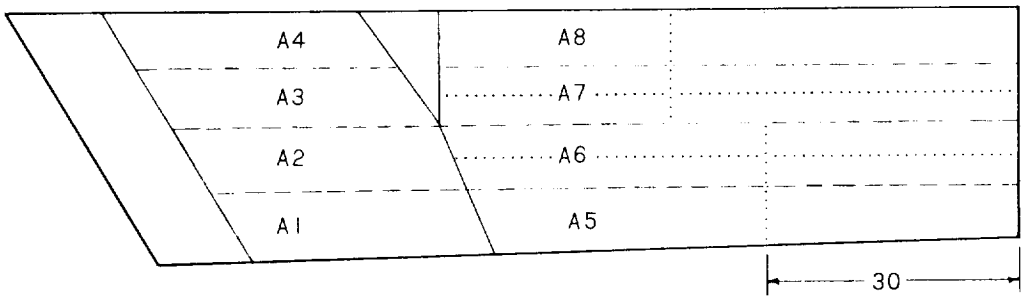

Right side

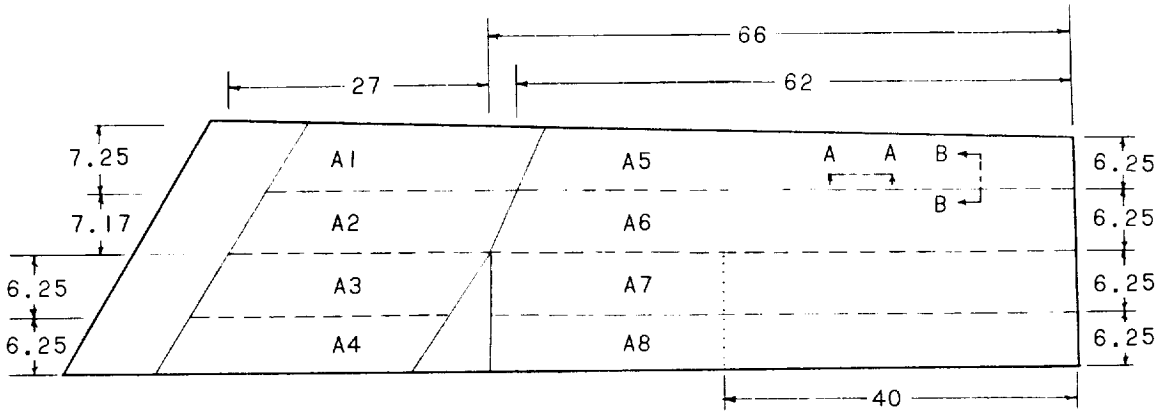

Left side

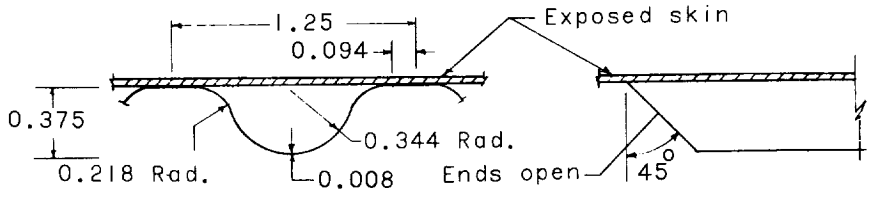

Section A—A Section B—B

Figure 2.- Nonrecoverable-stabilizer panel details. All dimensions are in inches.

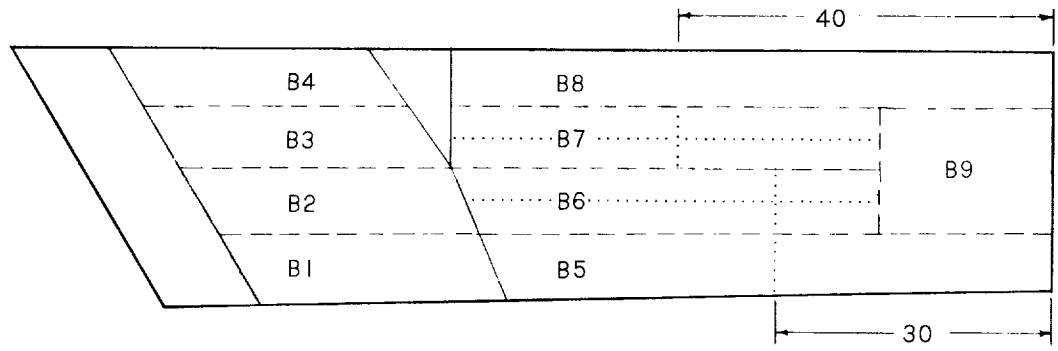

Right side

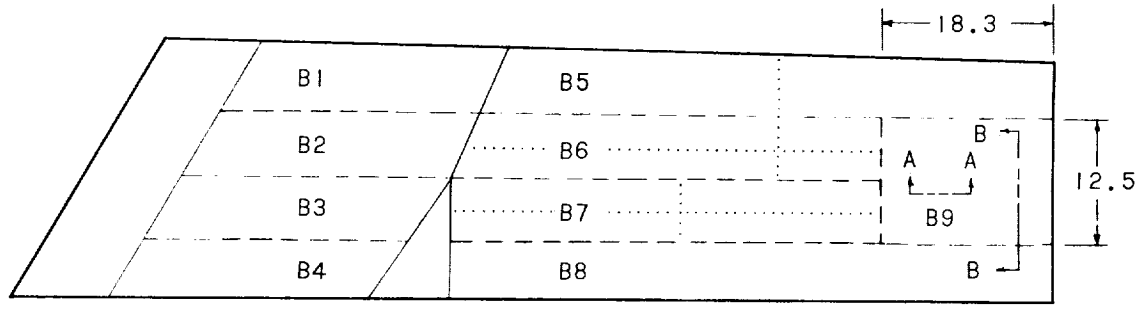

Left side

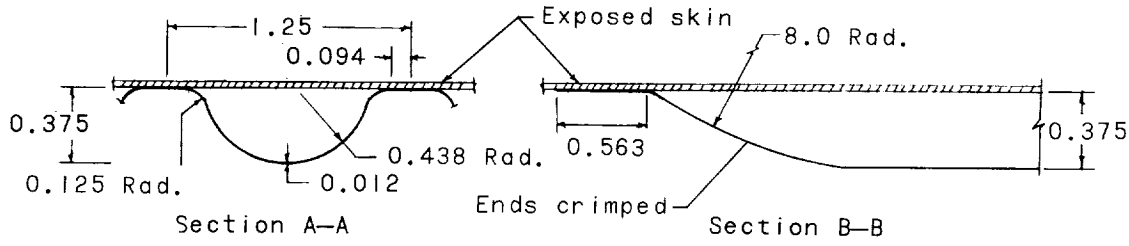

Figure 3.- Recoverable-stabilizer panel details. All dimensions are in inches.

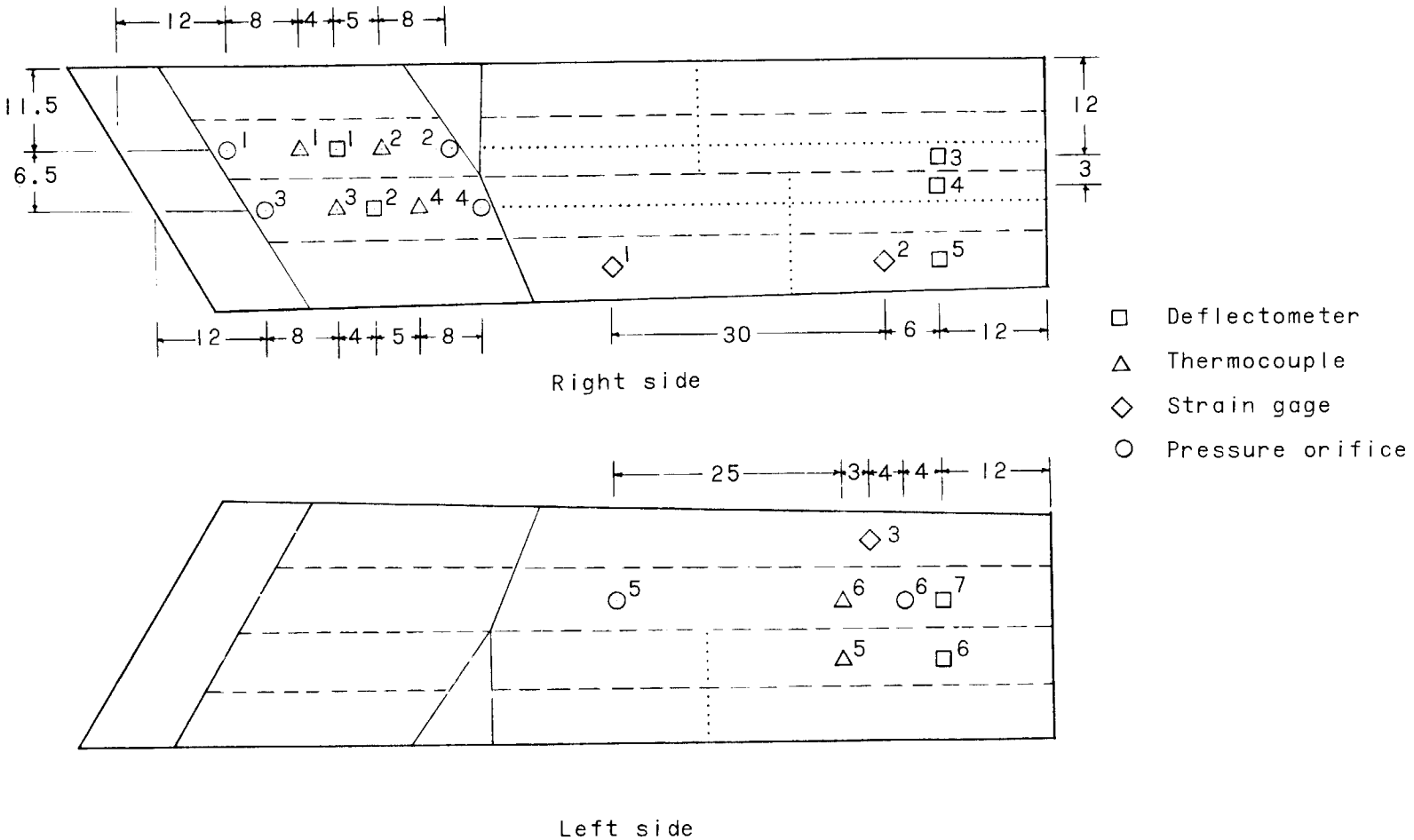

Figure 4.- Nonrecoverable-stabilizer instrumentation. All dimensions are in inches.

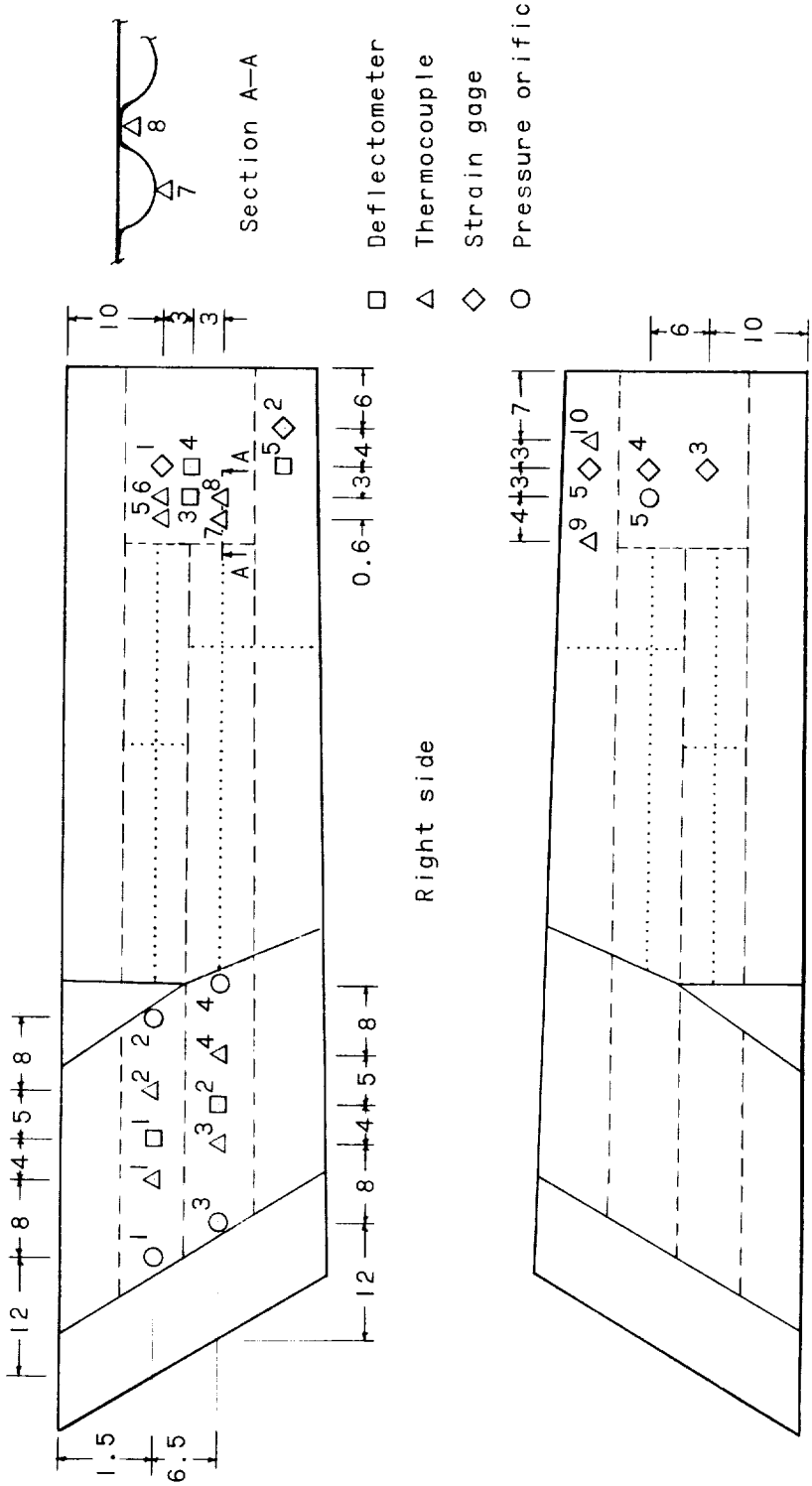

Figure 5.- Recoverable-stabilizer instrumentation. All dimensions are in inches.

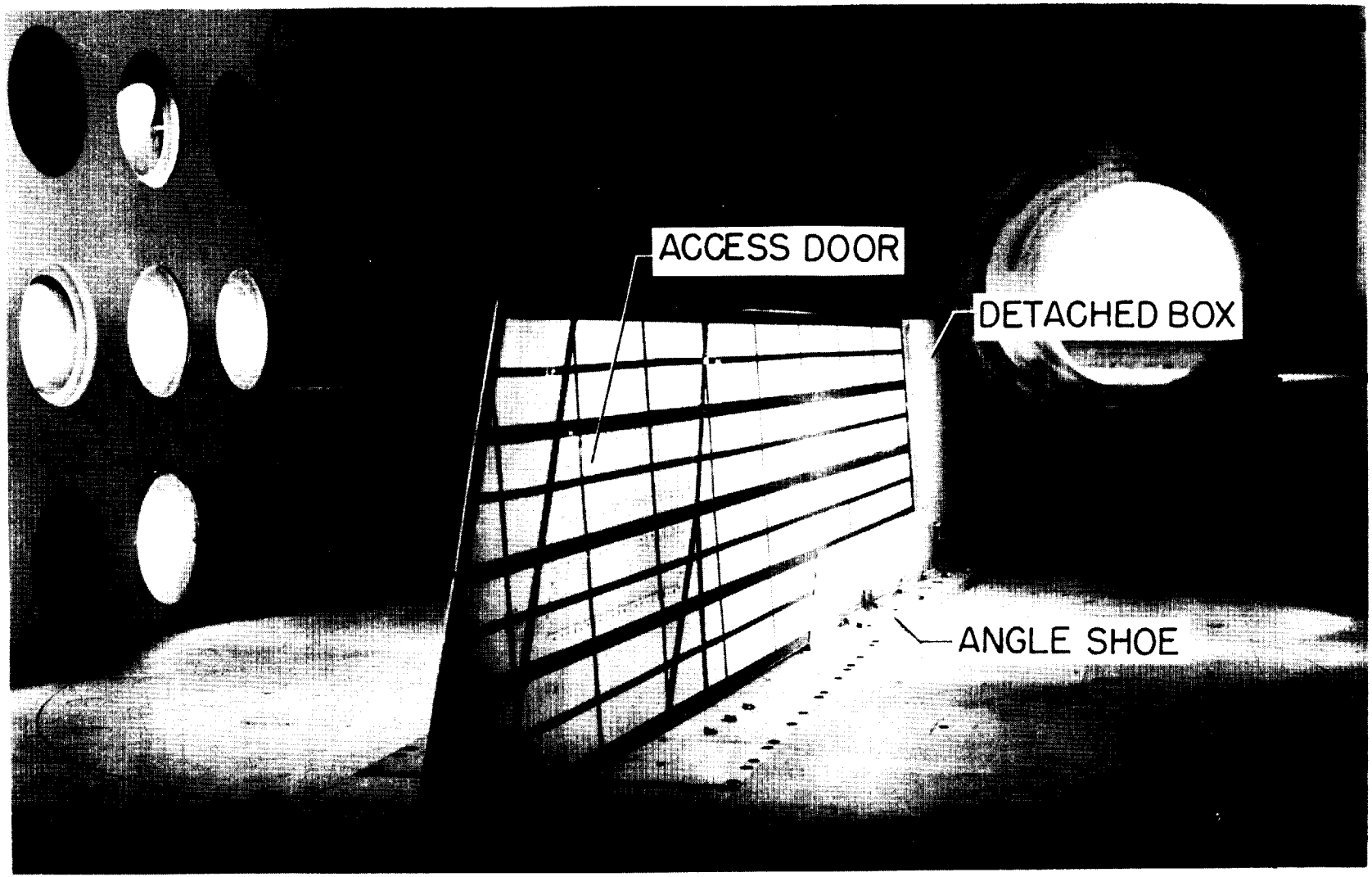

L-60-6522.1

Figure 6.- Nonrecoverable stabilizer of X-15 airplane mounted in test section (as viewed from upstream) showing angle shoe, detached box, and access doors.

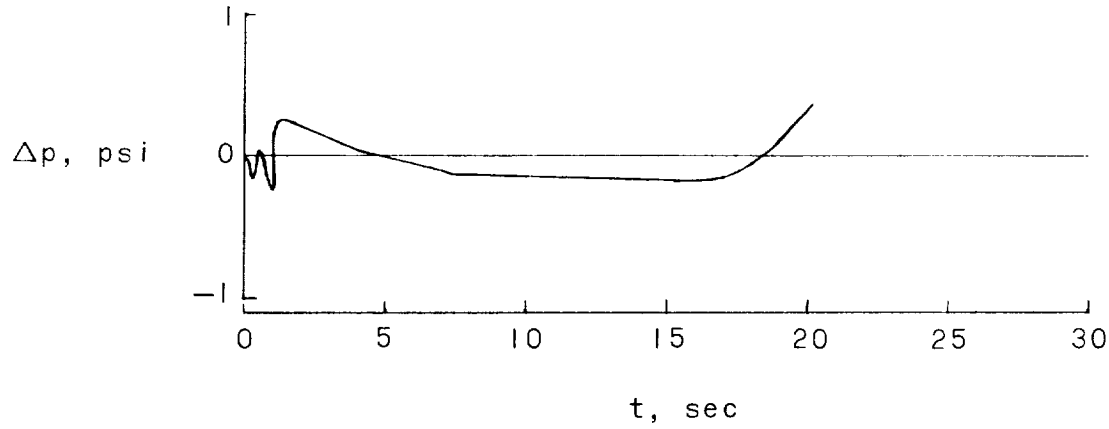

(a) Differential pressure (panel A6).

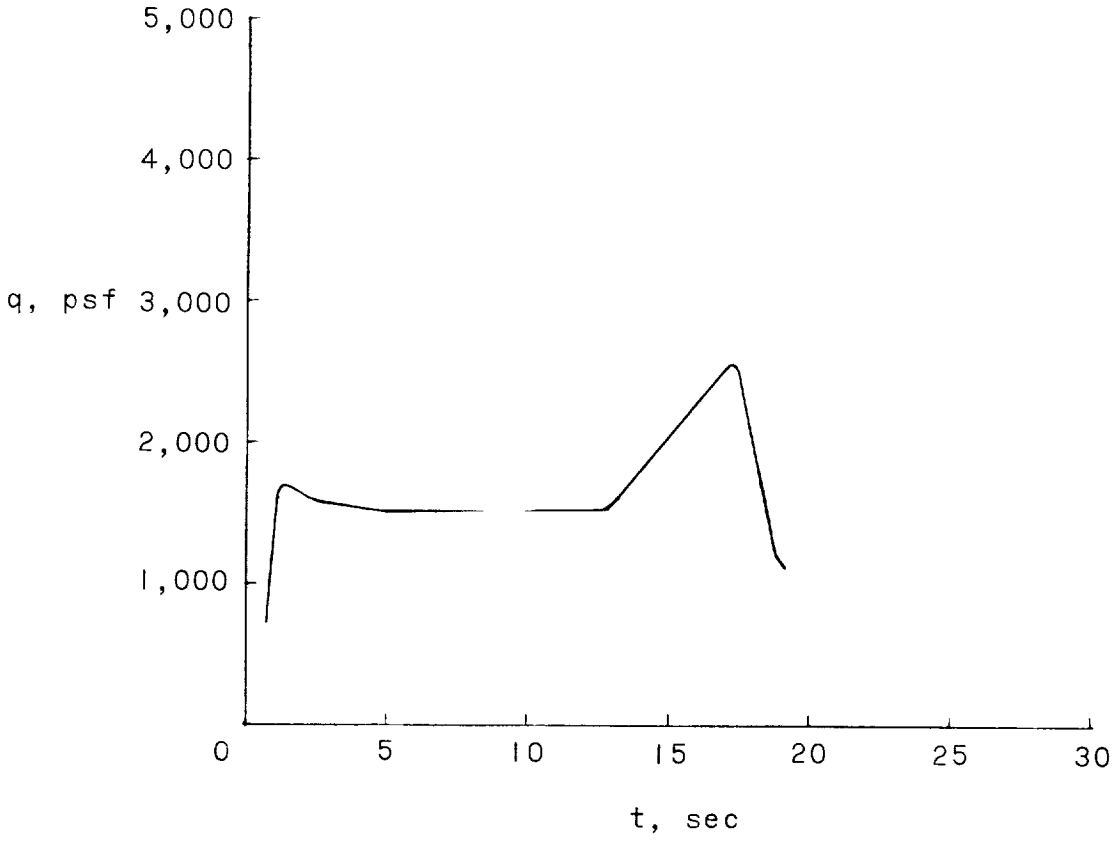

(b) Dynamic pressure.

Figure 7.- Pressure and temperature histories for the nonrecoverable stabilizer. (Test 1.)

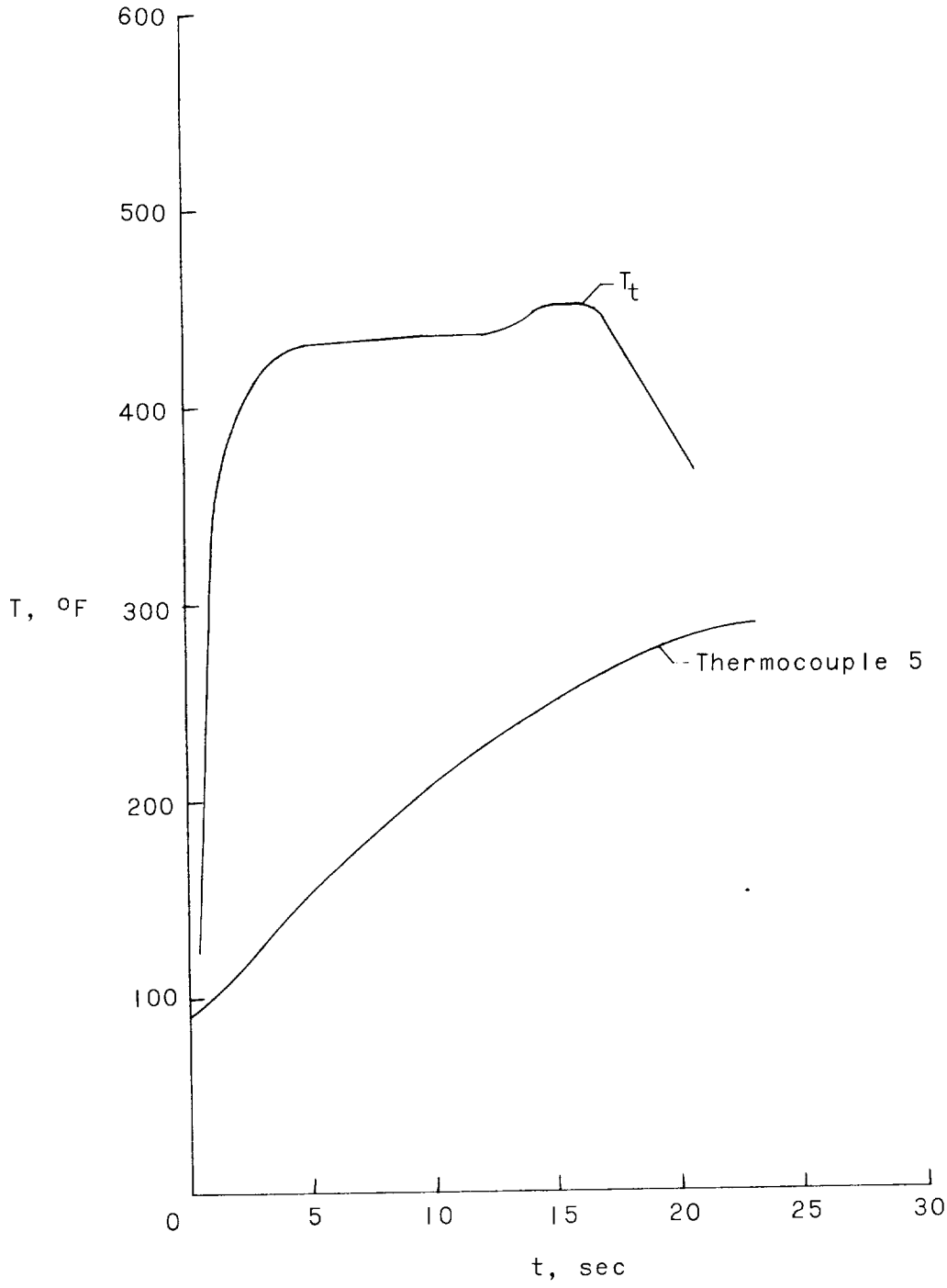

(c) Stagnation temperature and panel temperature.

Figure 7.- Concluded.

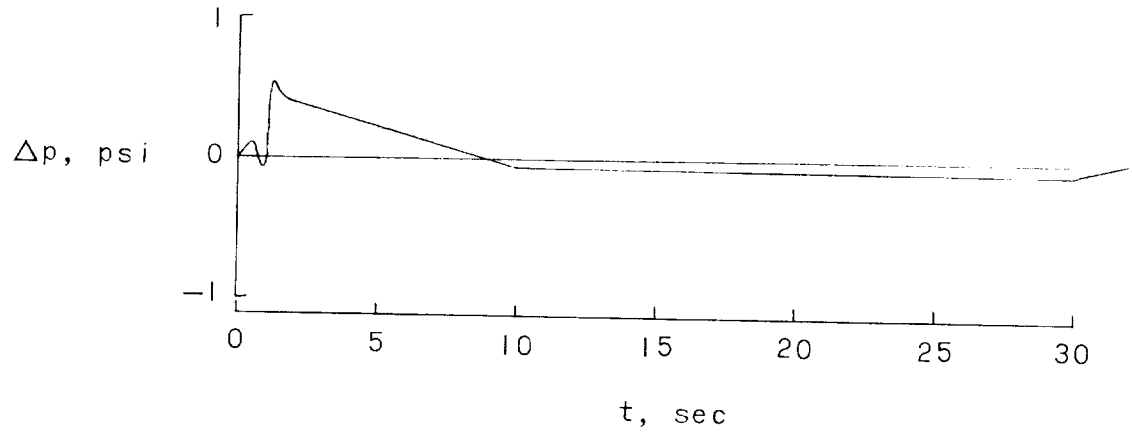

(a) Differential pressure (panel A6).

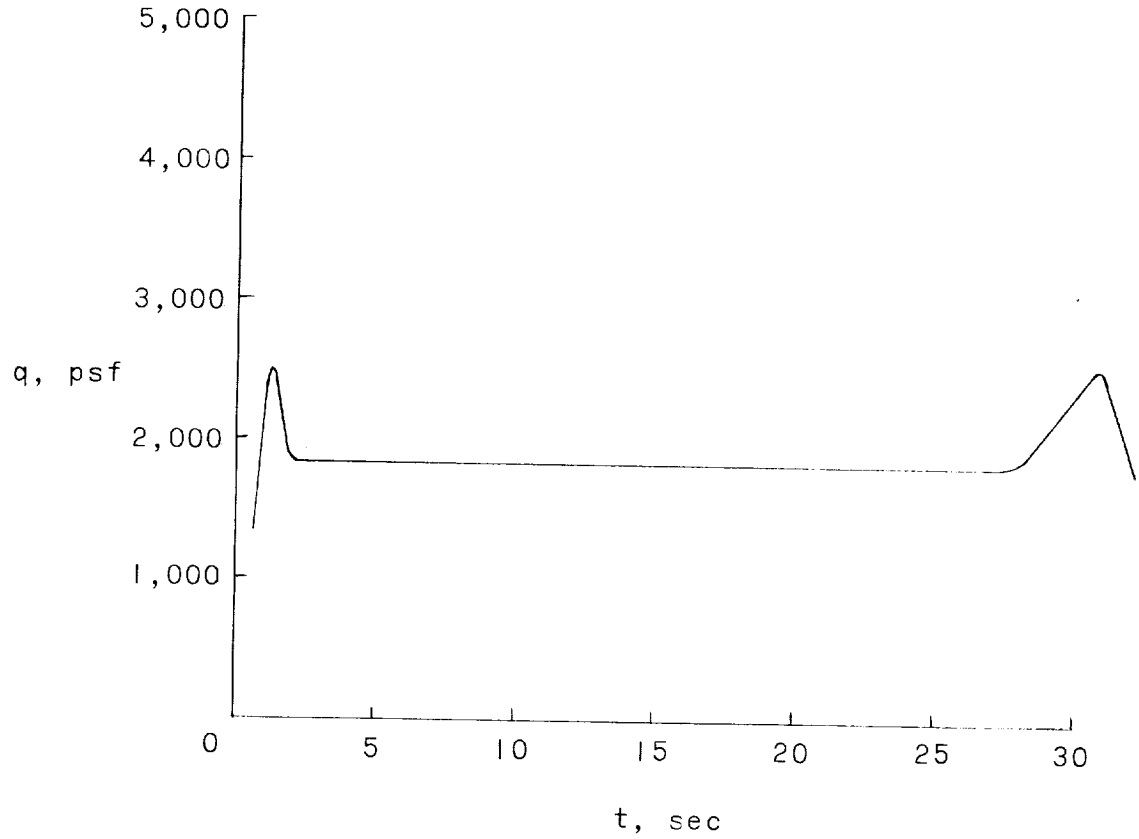

(b) Dynamic pressure.

Figure 8.- Pressure and temperature histories for the nonrecoverable stabilizer. (Test 2.)

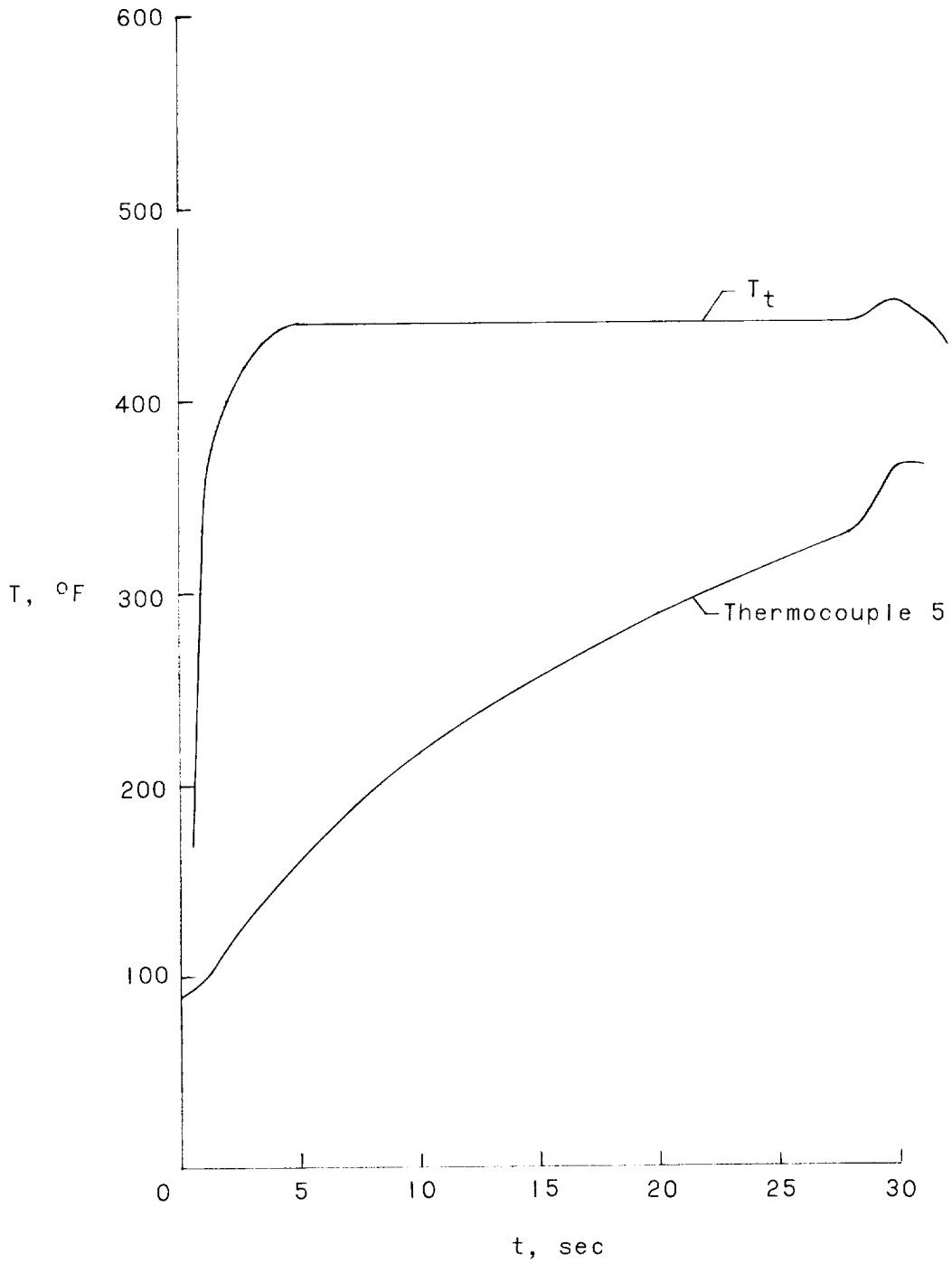

(c) Stagnation temperature and panel temperature.

Figure 8.- Concluded.

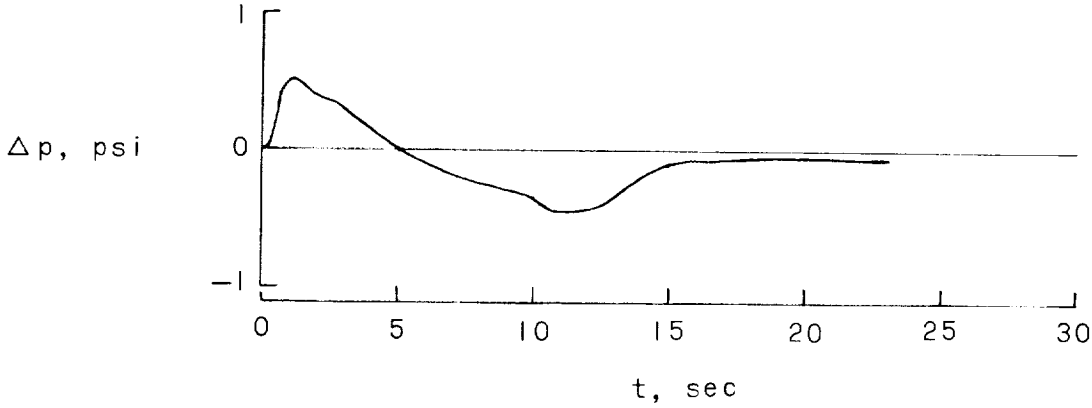

(a) Differential pressure (panel A6).

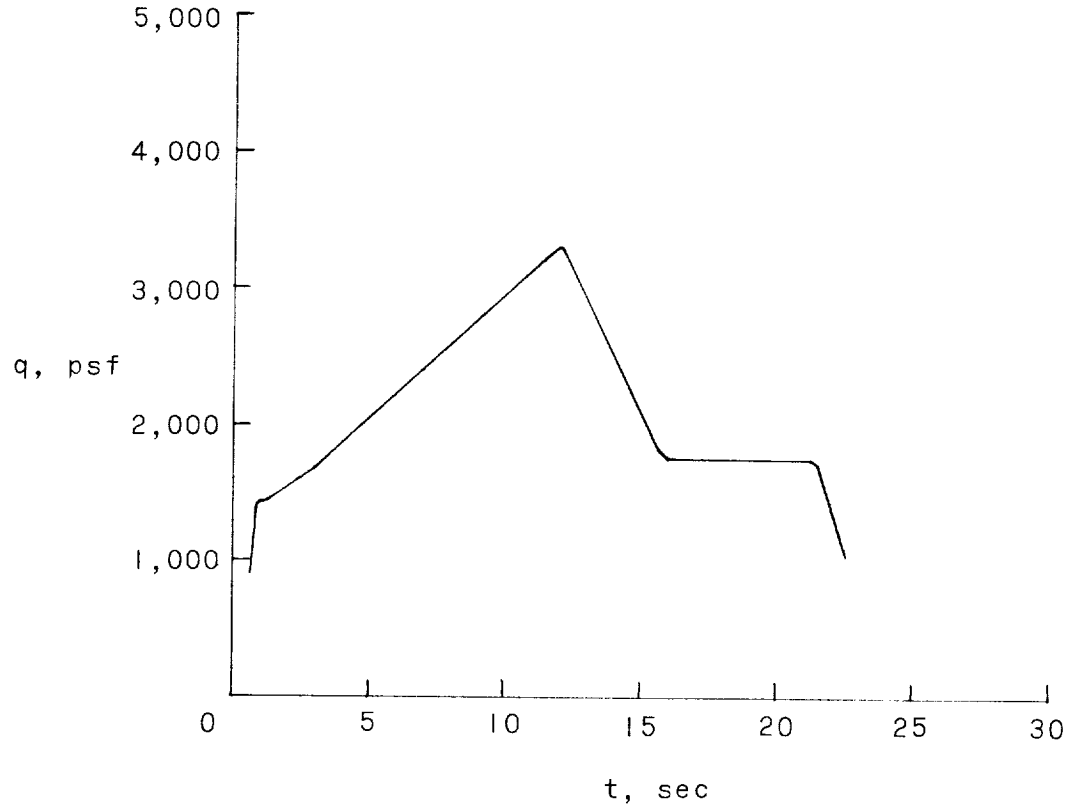

(b) Dynamic pressure.

Figure 9.- Pressure and temperature histories for the nonrecoverable stabilizer. (Test 3.)

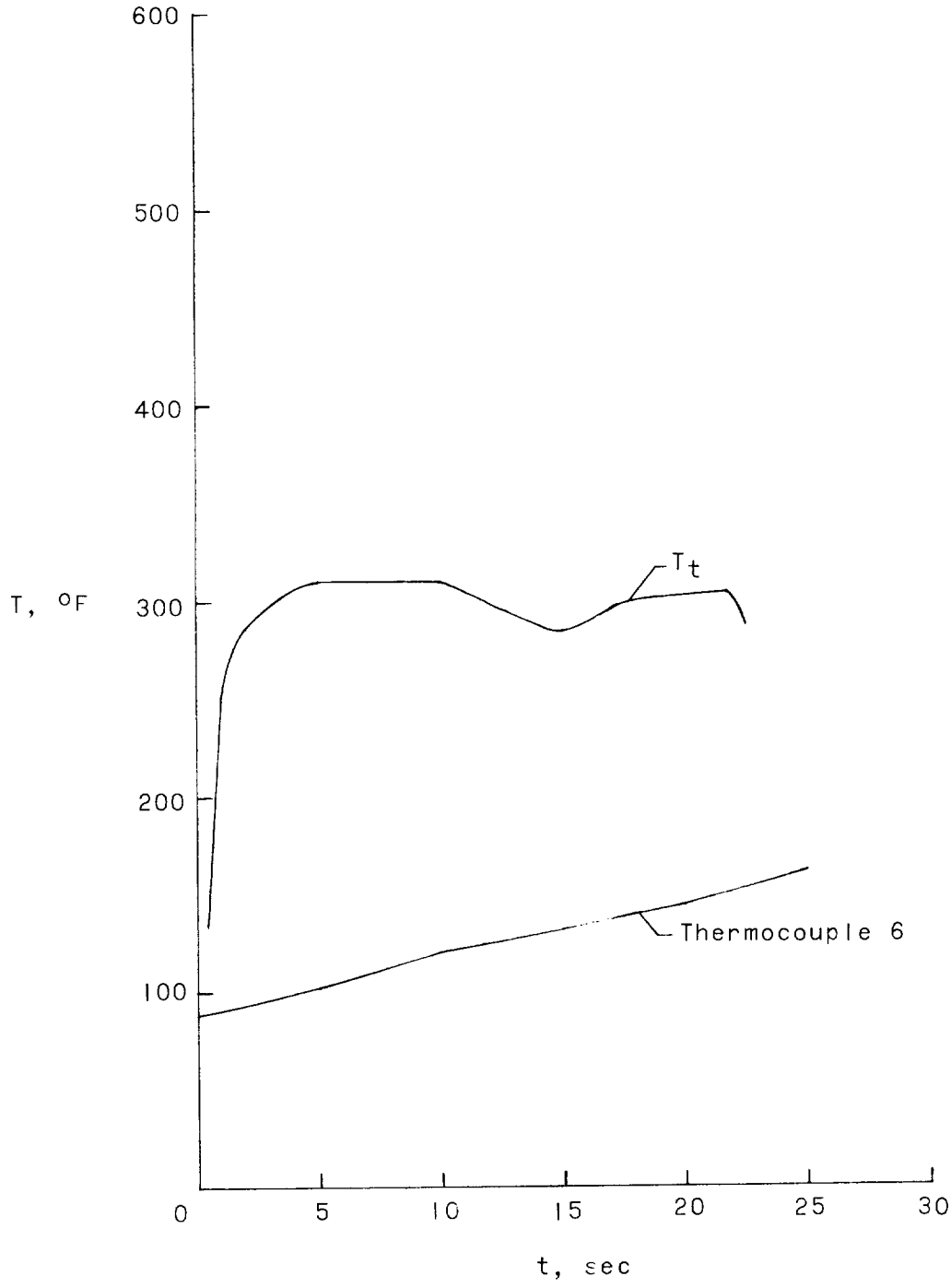

(c) Stagnation temperature and panel temperature.

Figure 9.- Concluded.

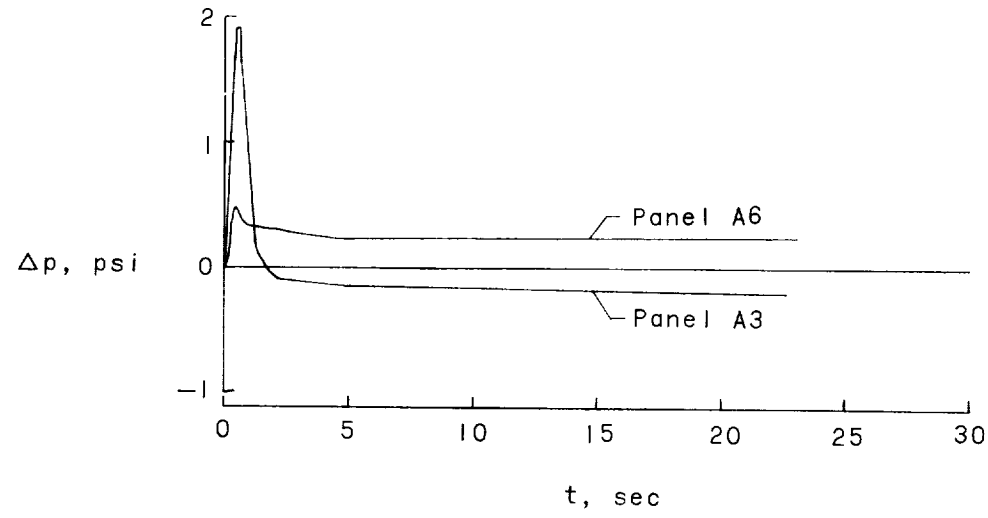

(a) Differential pressure.

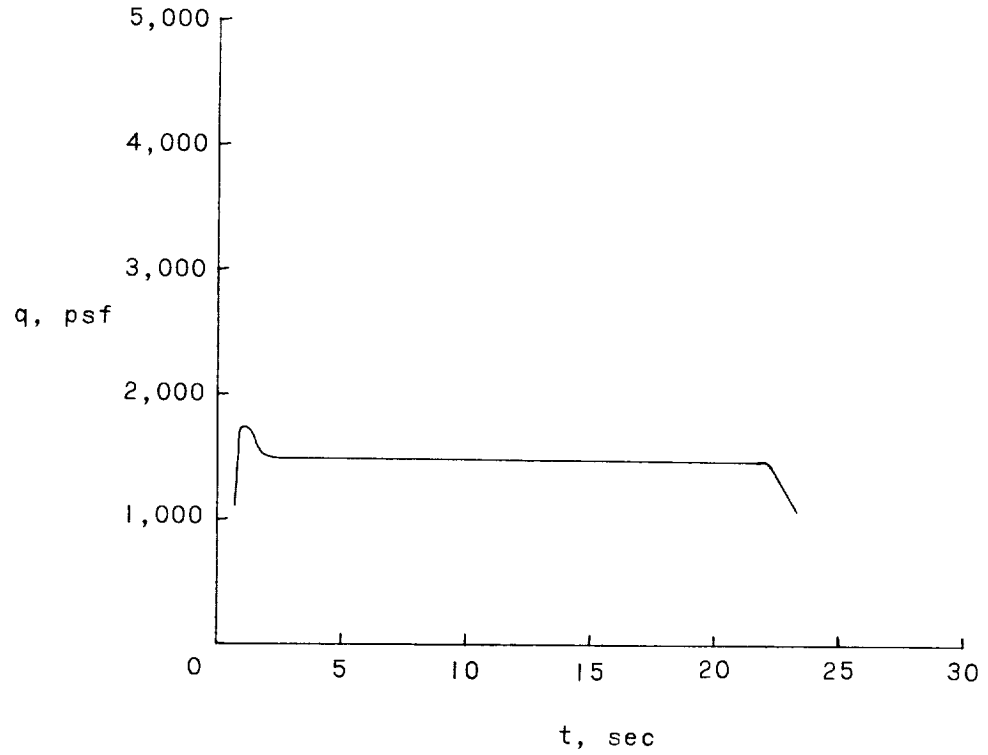

(b) Dynamic pressure.

Figure 10.- Pressure and temperature histories for the nonrecoverable stabilizer. (Test 4.)

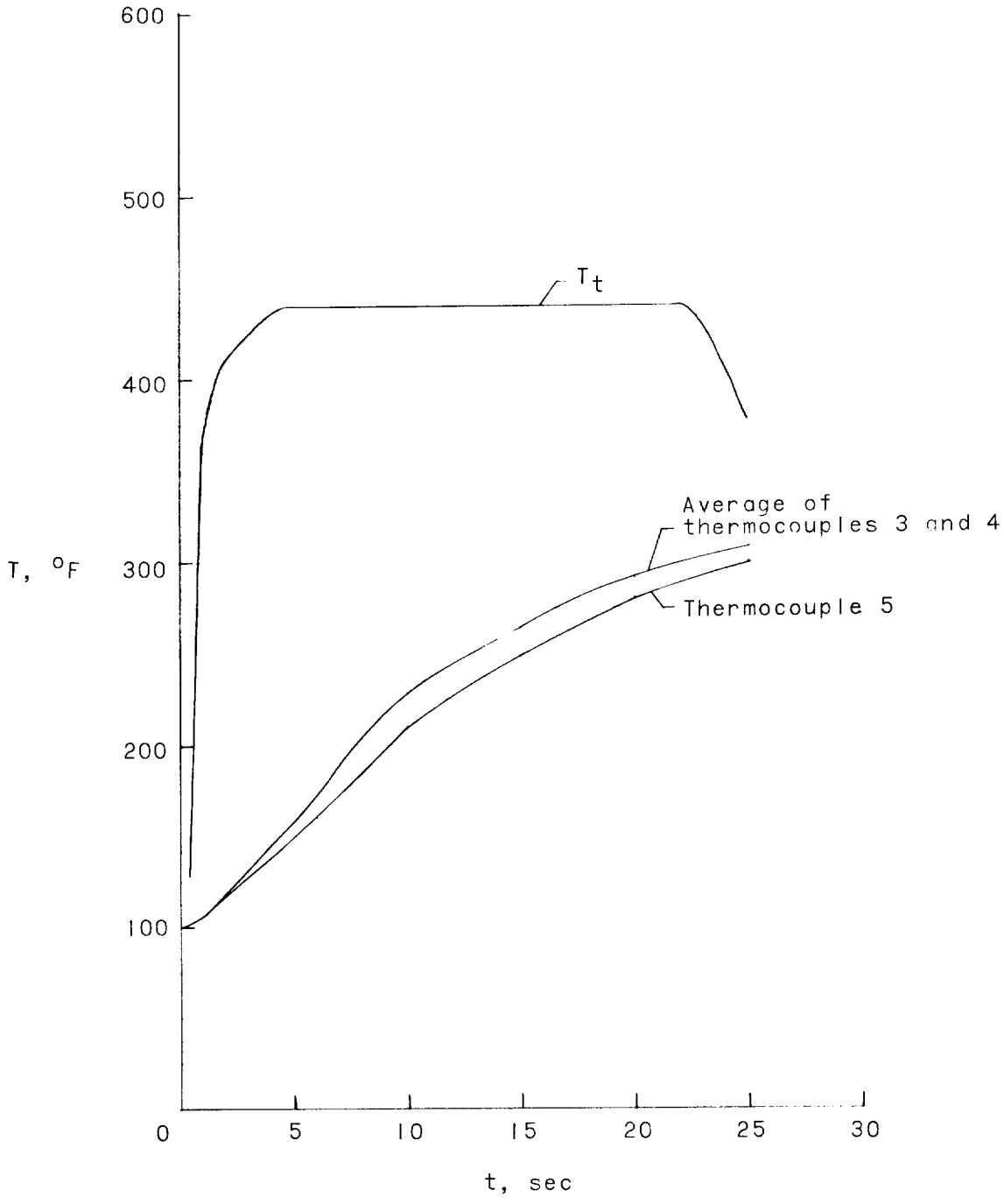

(c) Stagnation temperature and panel temperature.

Figure 10.- Concluded.

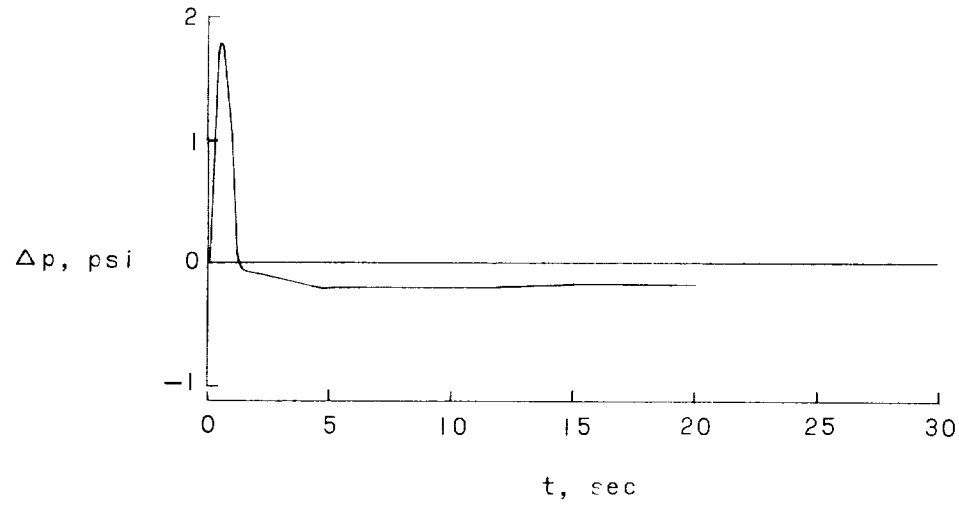

(a) Differential pressure (panel A3).

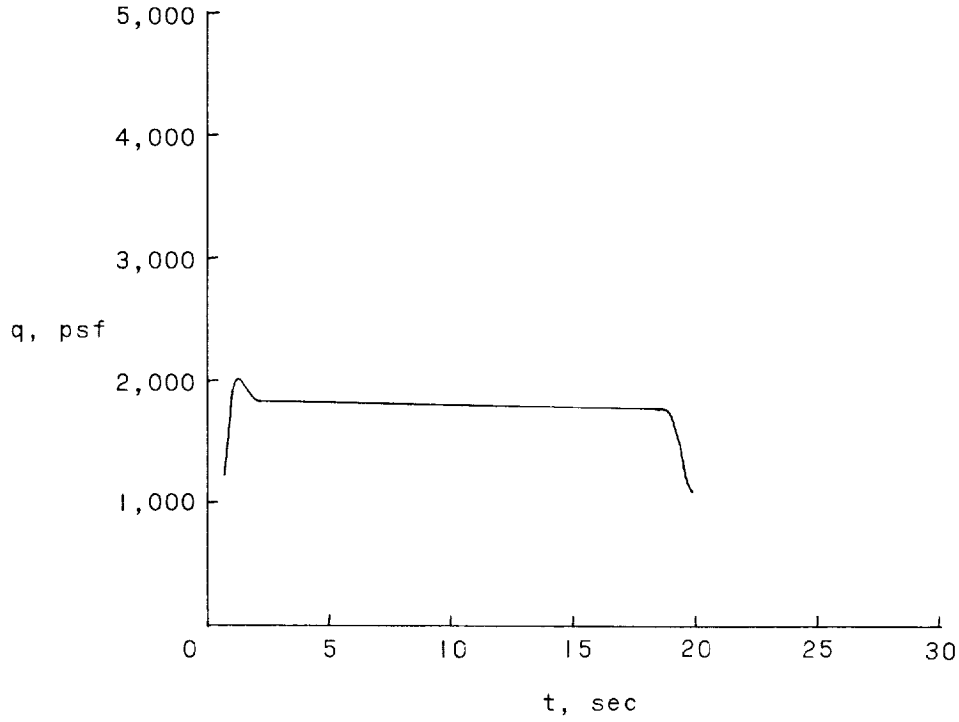

(b) Dynamic pressure.

Figure 11.- Pressure and temperature histories for the nonrecoverable stabilizer. (Test 5.)

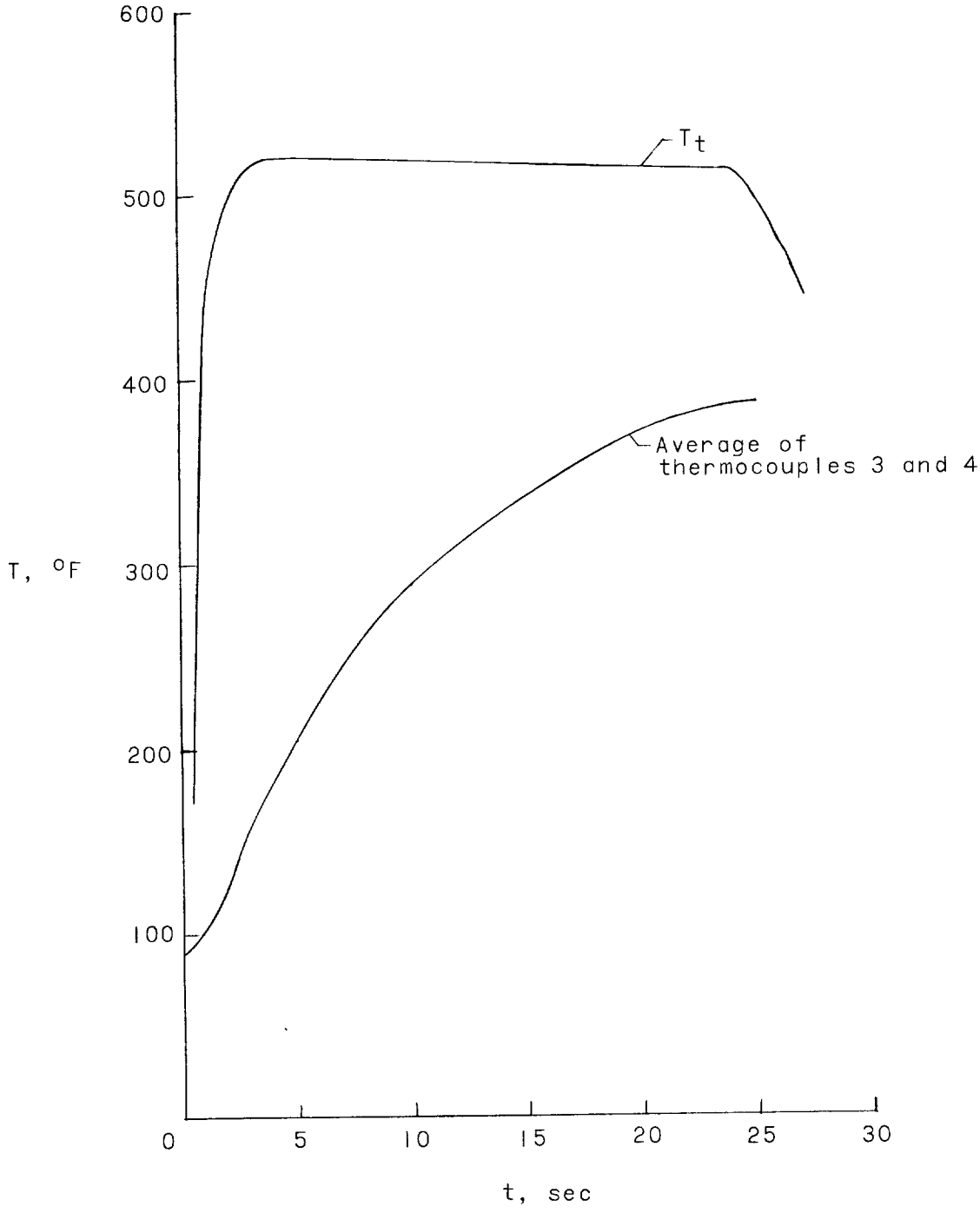

(c) Stagnation temperature and panel temperature.

Figure 11.- Concluded.

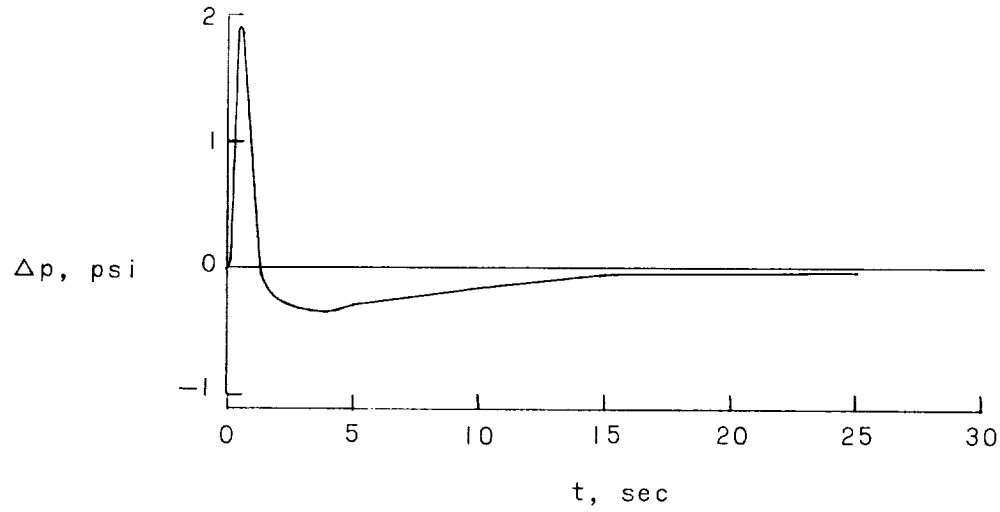

(a) Differential pressure (panel A3).

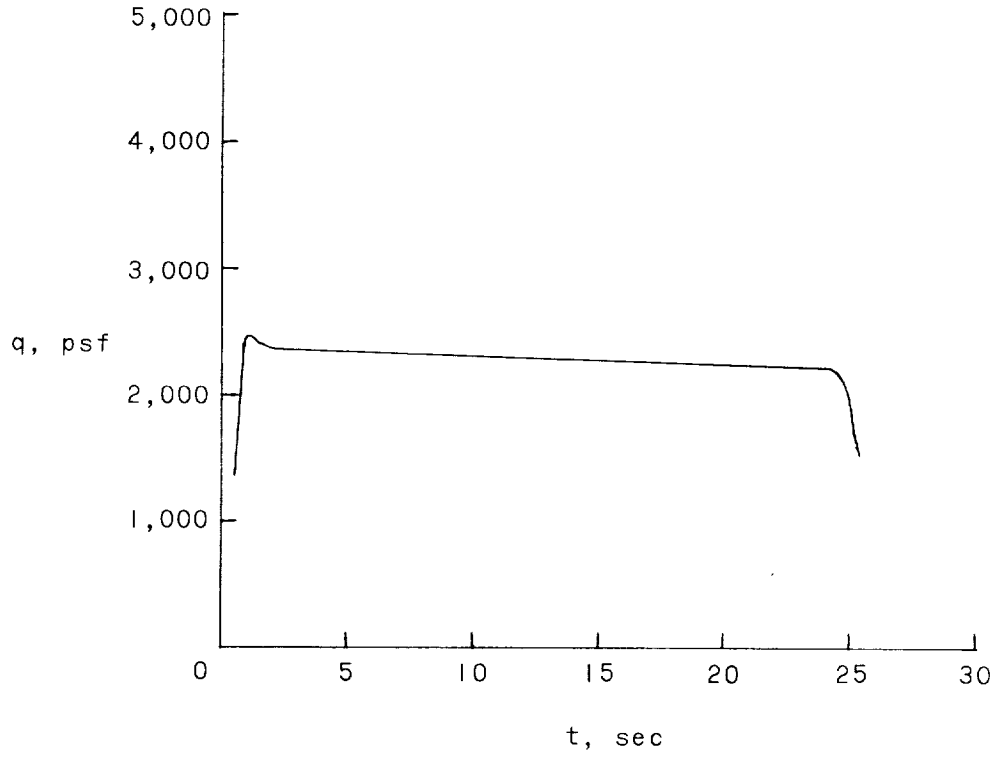

(b) Dynamic pressure.

Figure 12.- Pressure and temperature histories for the nonrecoverable stabilizer. (Test 6.)

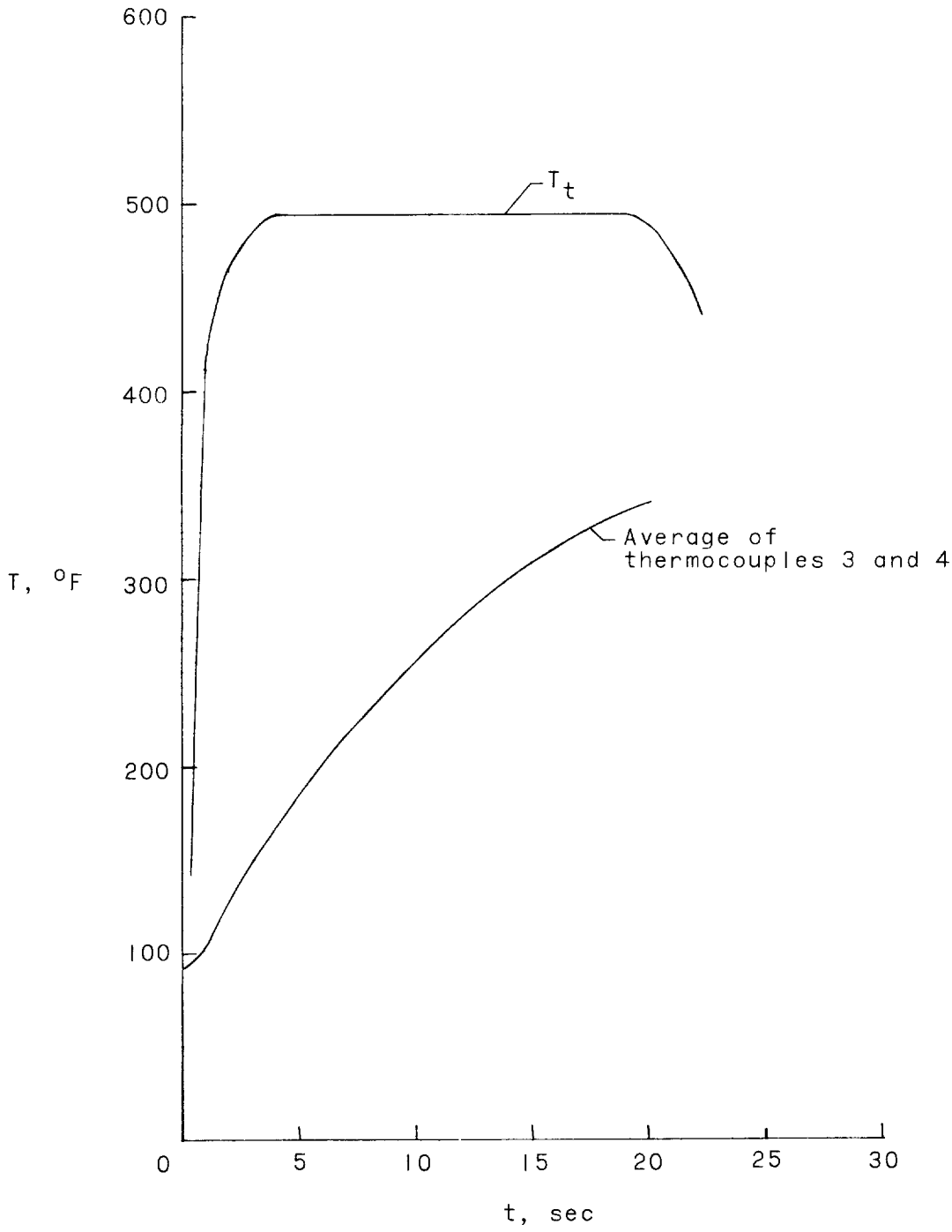

(c) Stagnation temperature and panel temperature.

Figure 12.- Concluded.

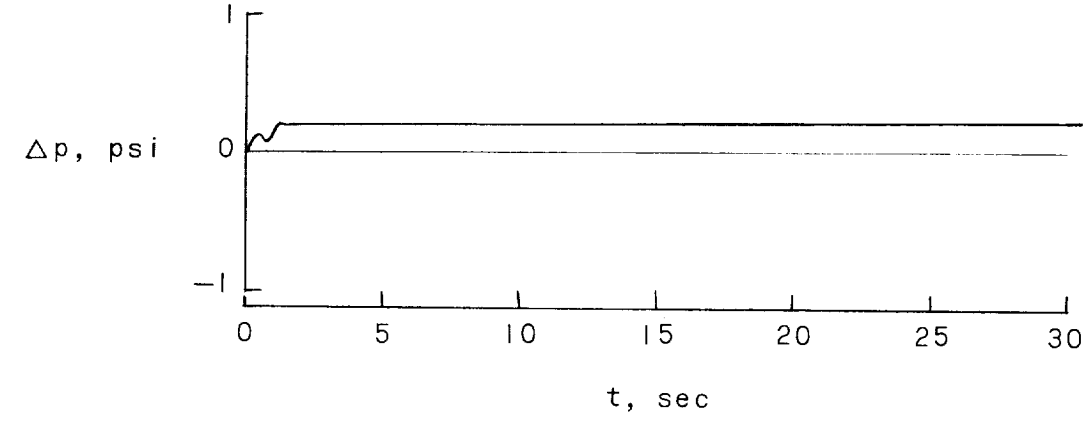

(a) Differential pressure (panel A6).

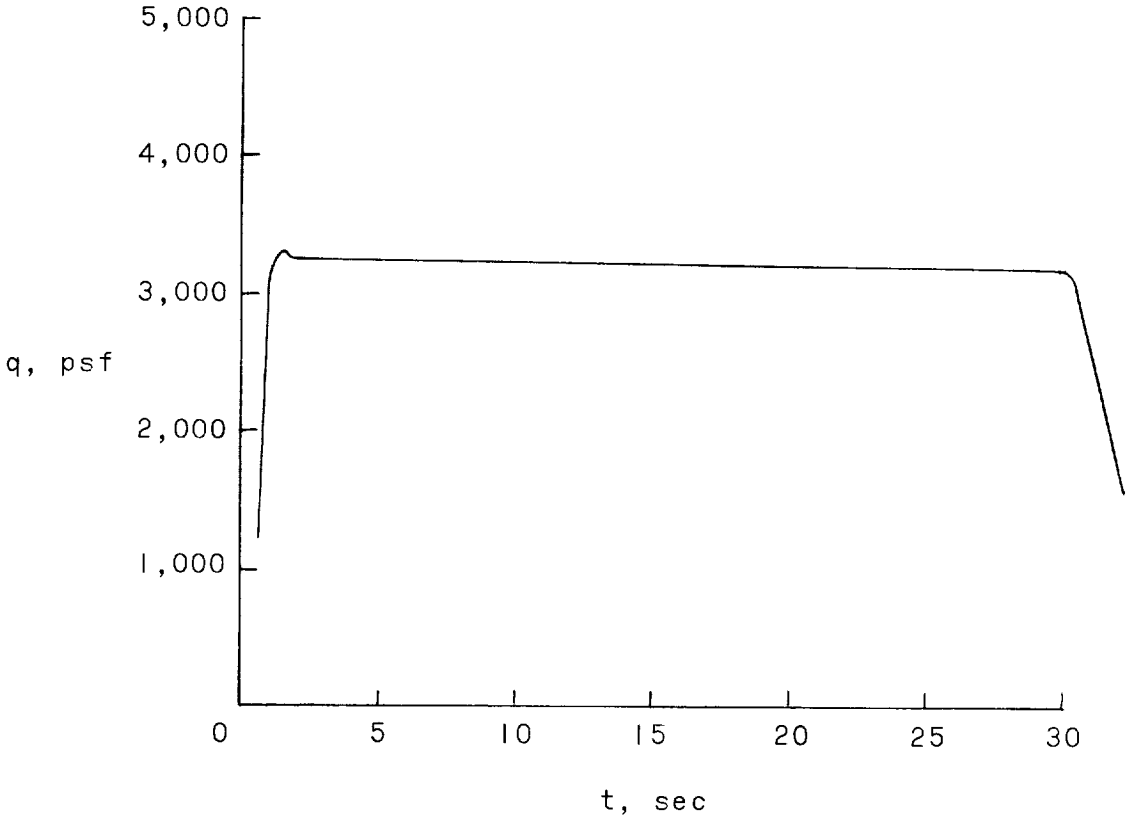

(b) Dynamic pressure.

Figure 13.- Pressure and temperature histories for the nonrecoverable stabilizer. (Test 7.)

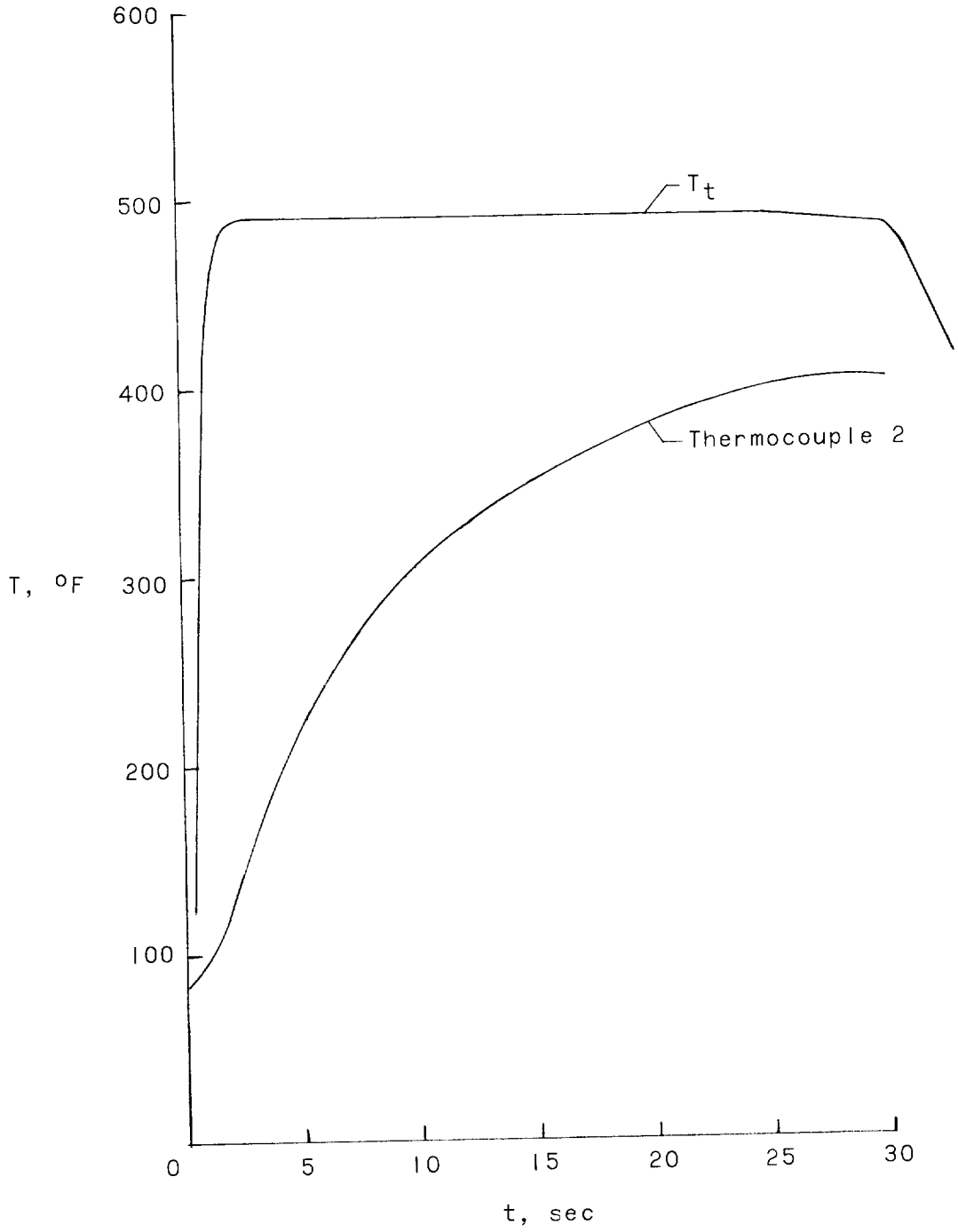

(c) Stagnation temperature and panel temperature.

Figure 13.- Concluded.

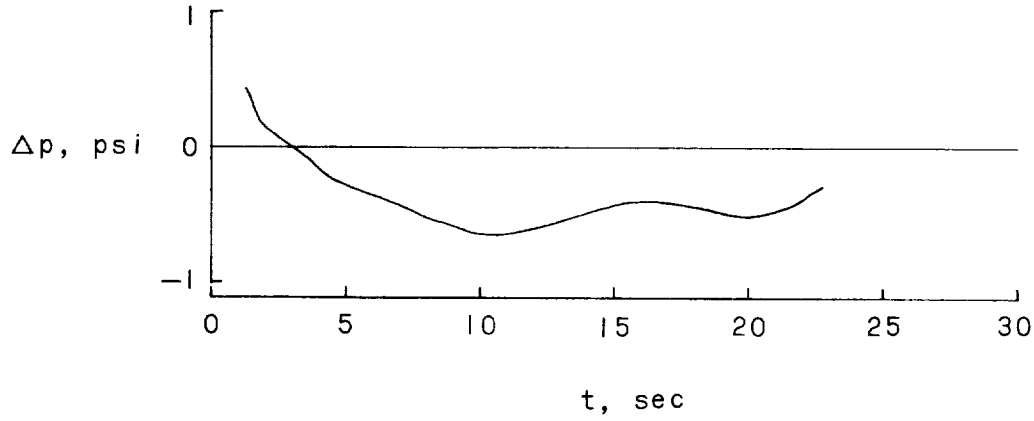

(a) Differential pressure (panel B9).

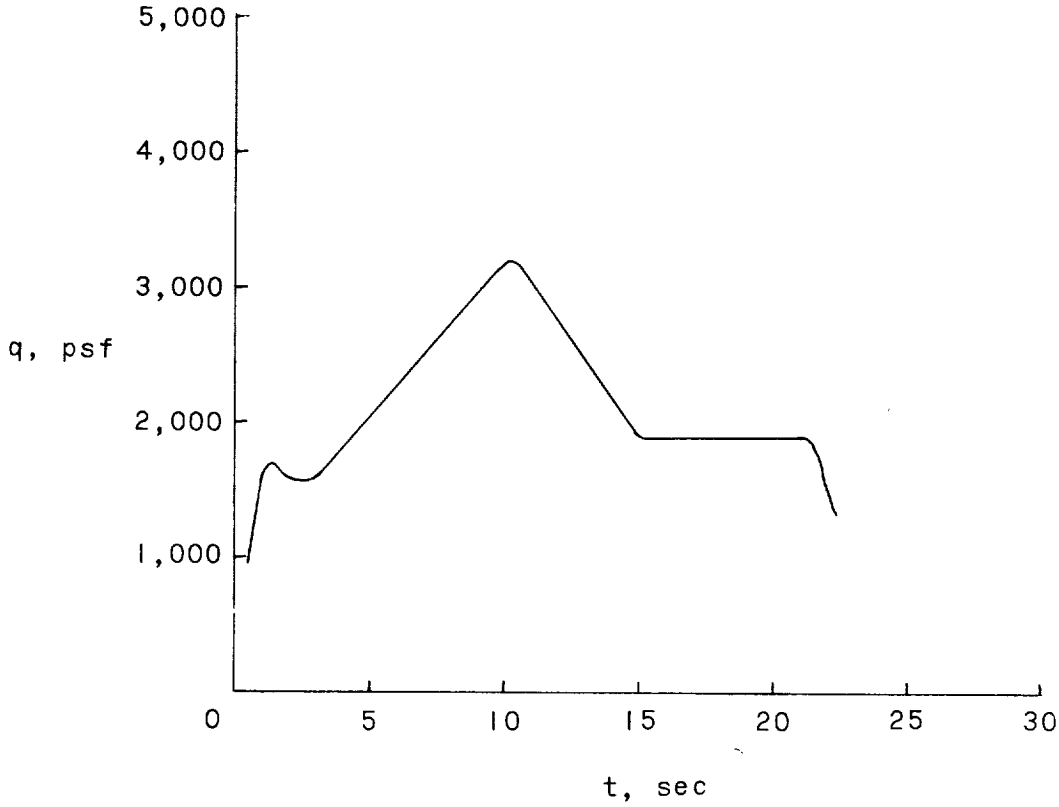

(b) Dynamic pressure.

Figure 14.- Pressure and temperature histories for the recoverable stabilizer. (Test 8.)

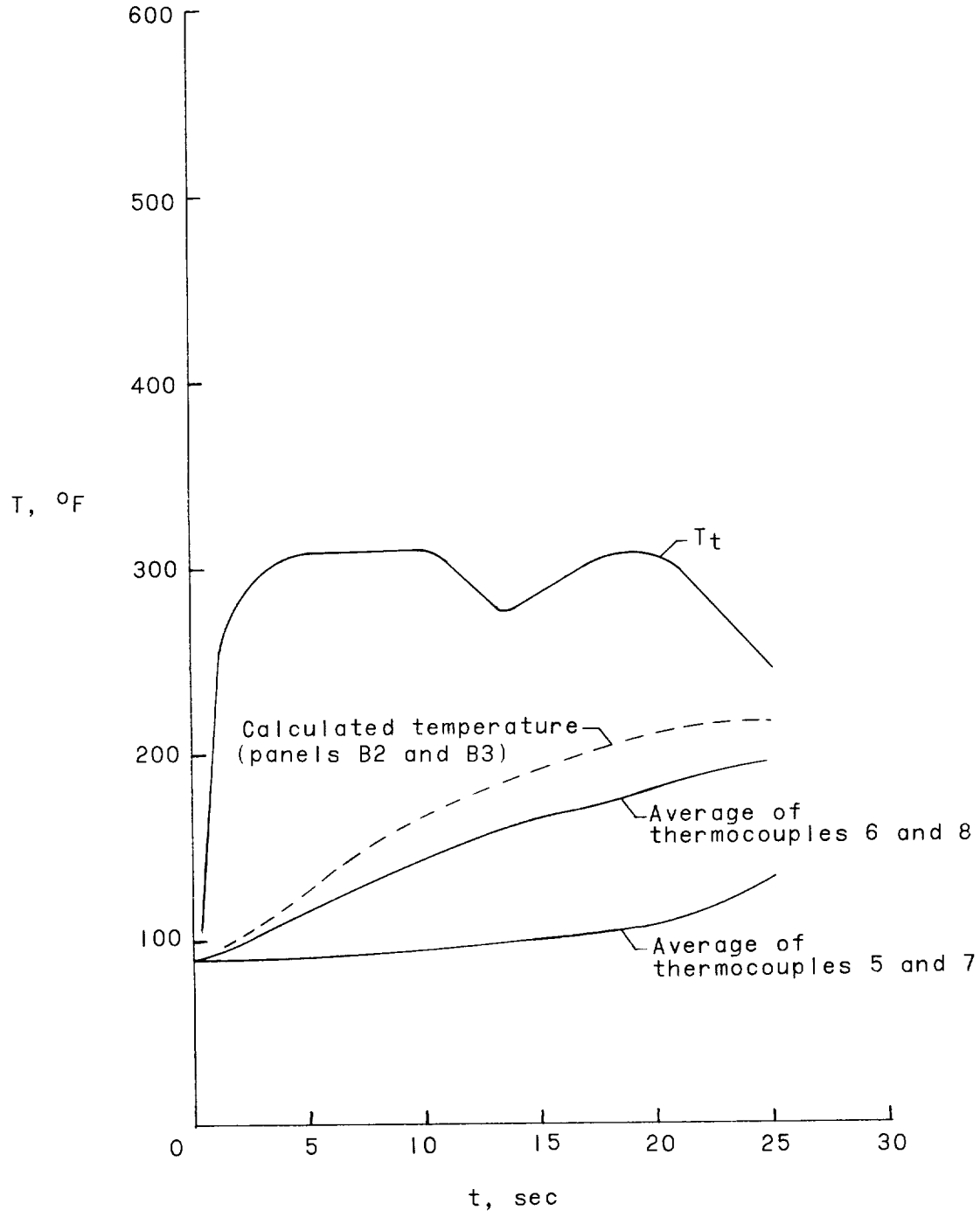

(c) Stagnation temperature and panel temperature.

Figure 14.- Concluded.

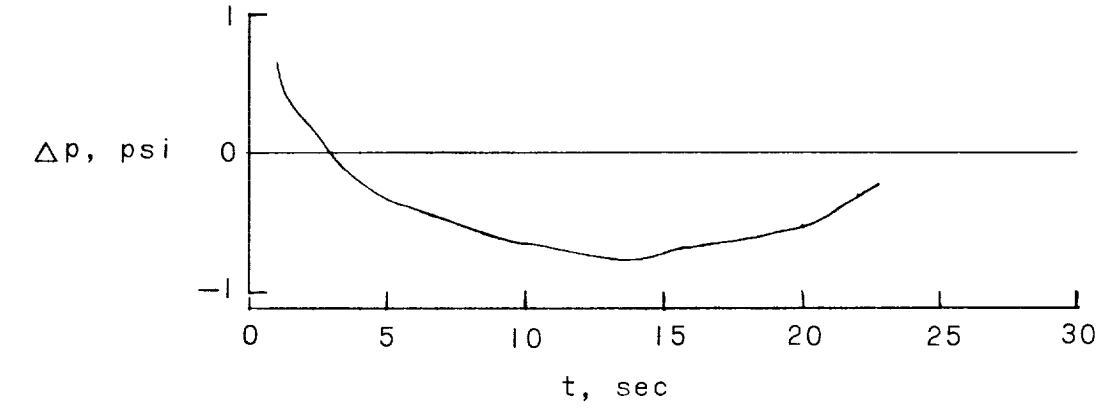

(a) Differential pressure (panel B9).

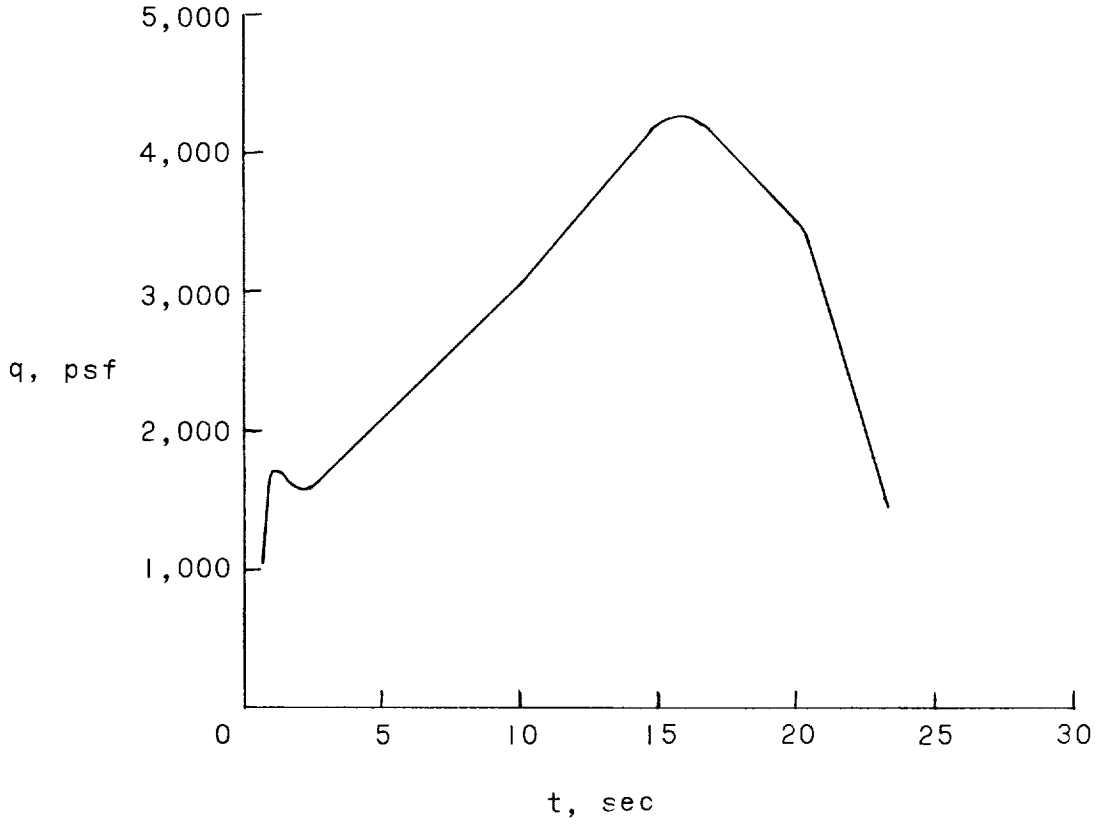

(b) Dynamic pressure.

Figure 15.- Pressure and temperature histories for the recoverable stabilizer. (Test 9.)

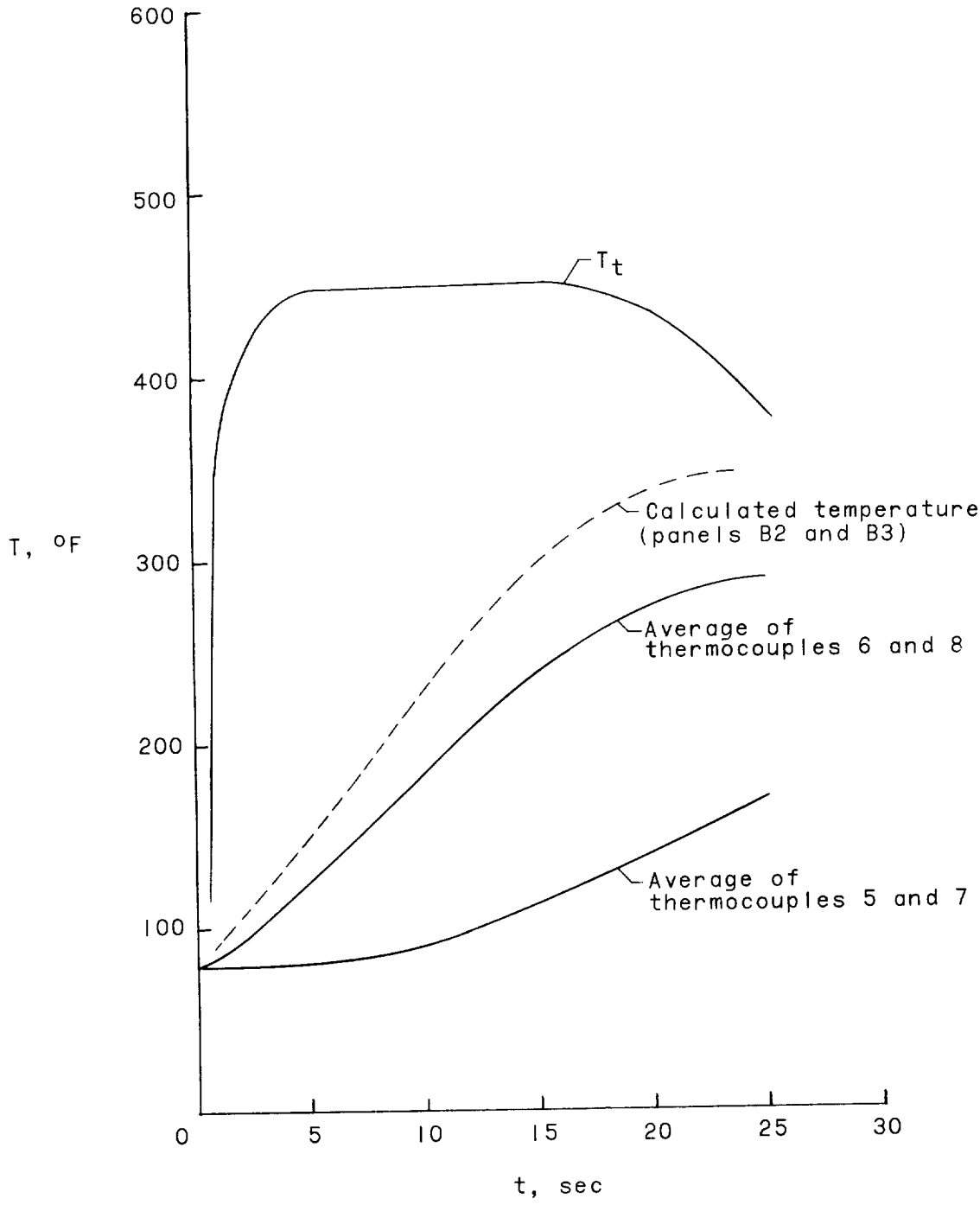

(c) Stagnation temperature and panel temperature.

Figure 15.- Concluded.

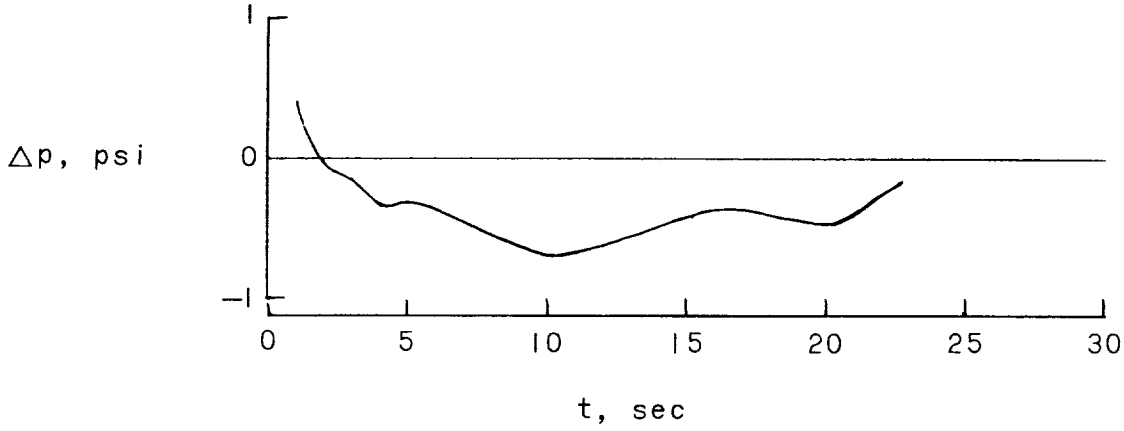

(a) Differential pressure (panel B9).

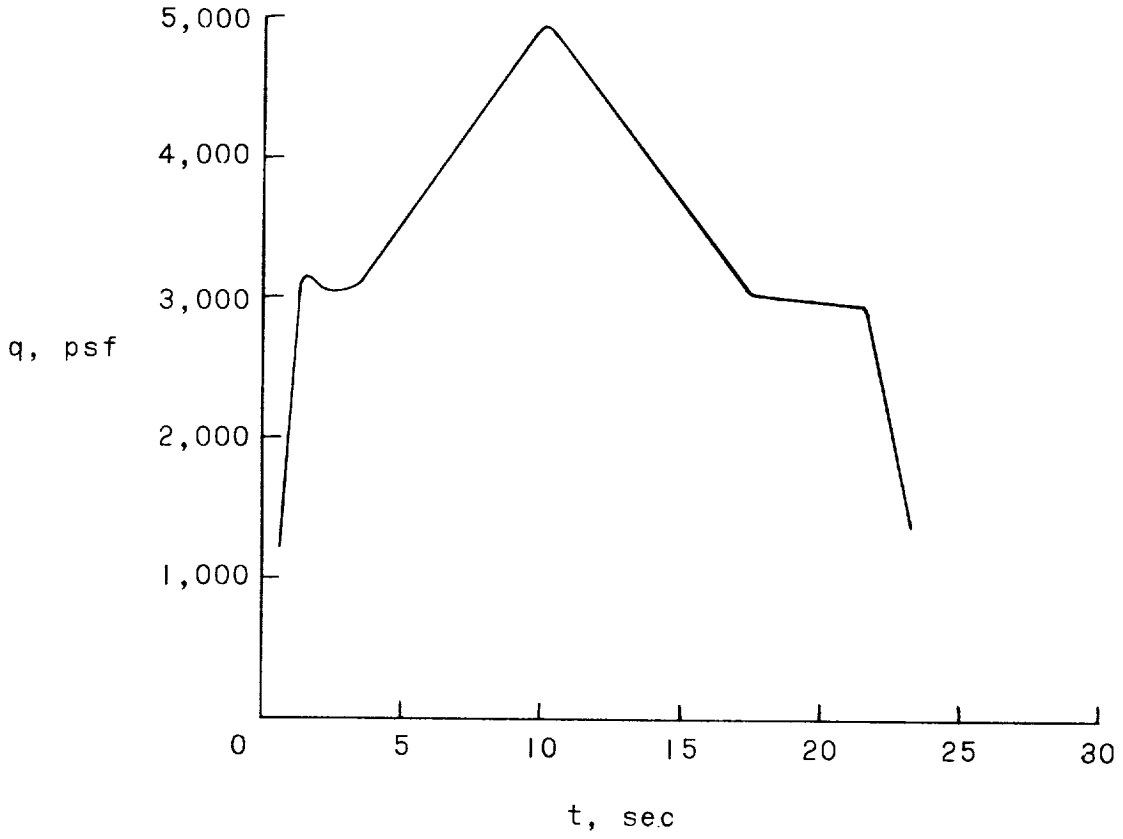

(b) Dynamic pressure.

Figure 16.- Pressure and temperature histories for the recoverable stabilizer. (Test 10.)

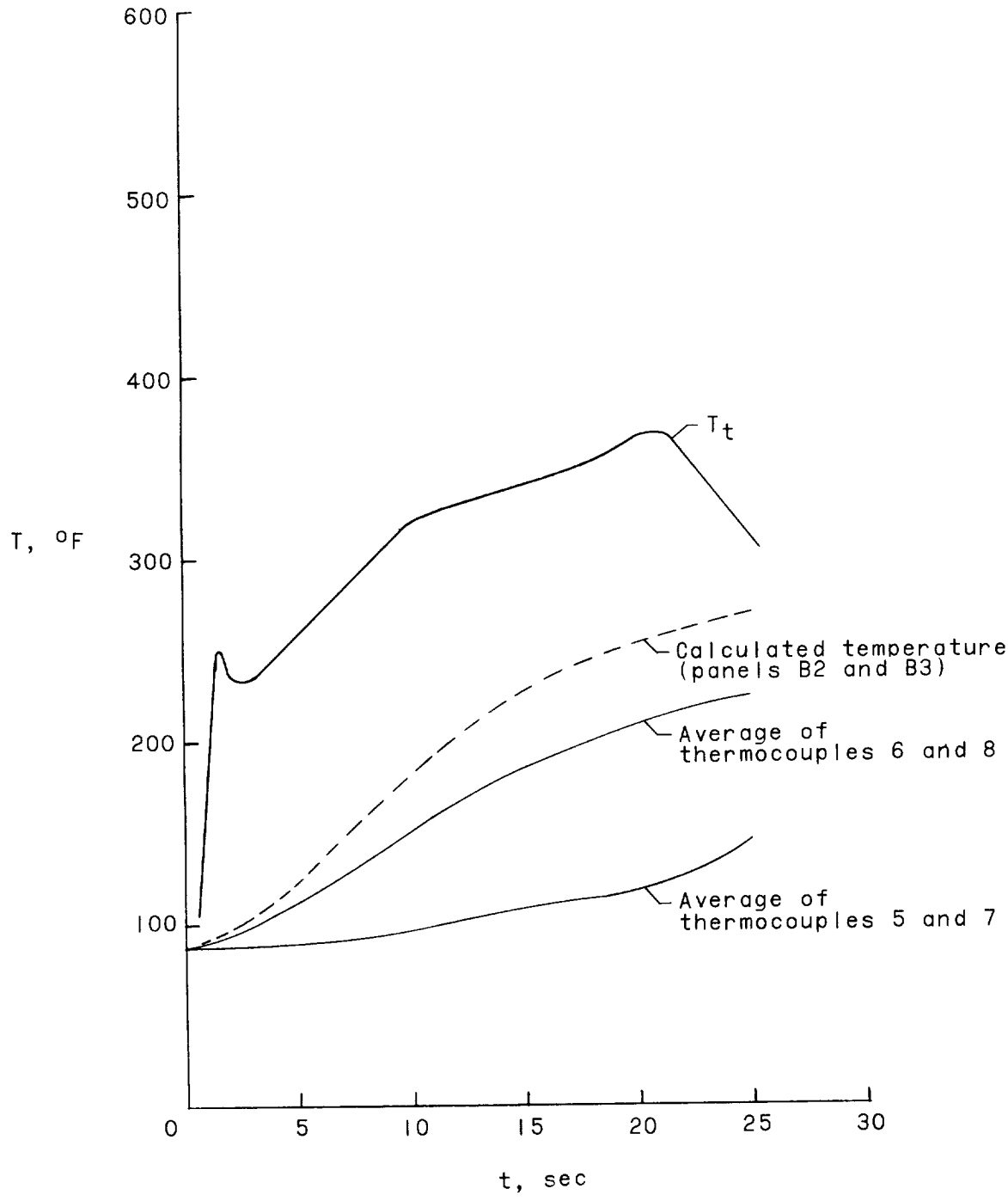

(c) Stagnation temperature and panel temperature.

Figure 16.- Concluded.

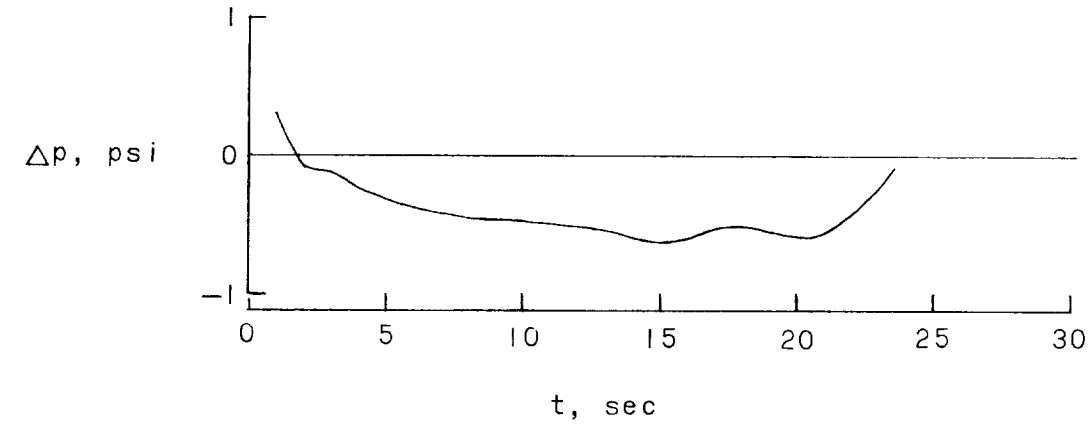

(a) Differential pressure (panel B9).

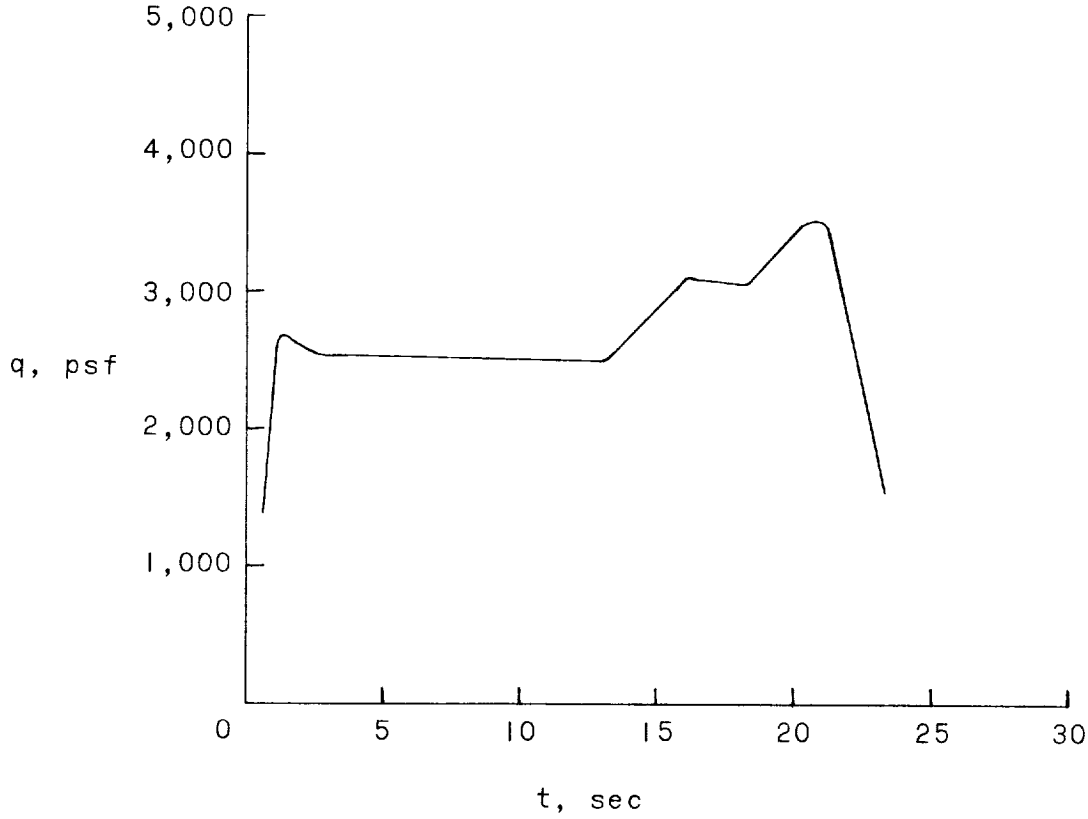

(b) Dynamic pressure.

Figure 17.- Pressure and temperature histories for the recoverable stabilizer. (Test 11.)

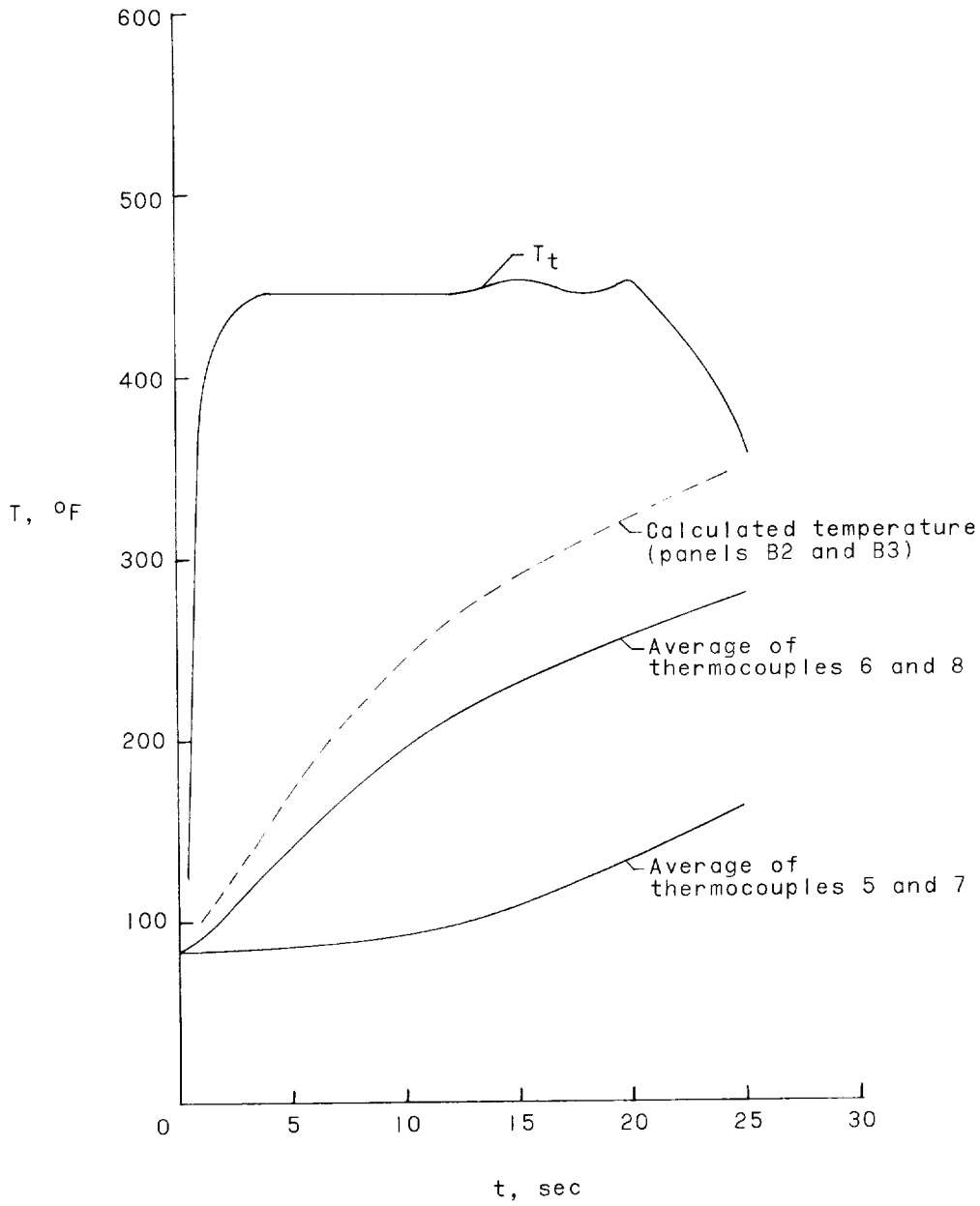

(c) Stagnation temperature and panel temperature.

Figure 17.- Concluded.

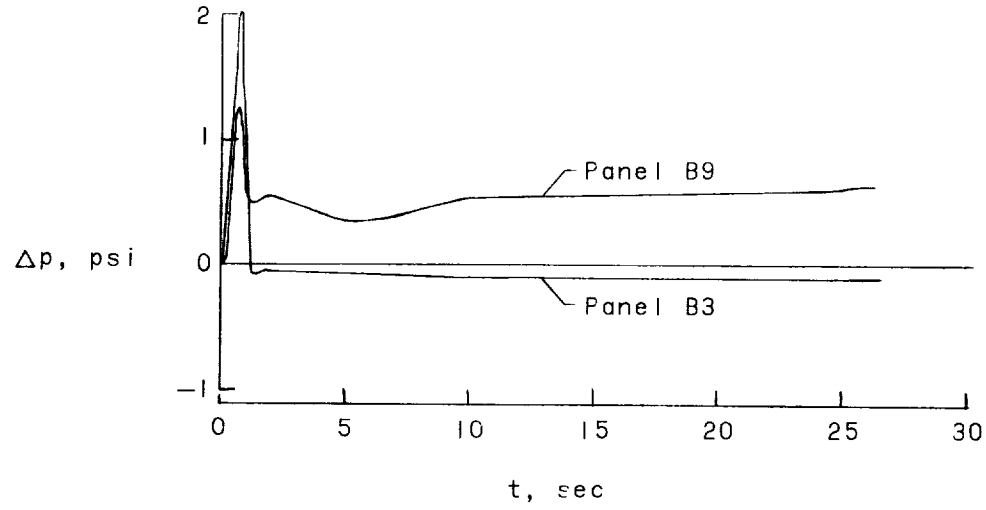

(a) Differential pressure.

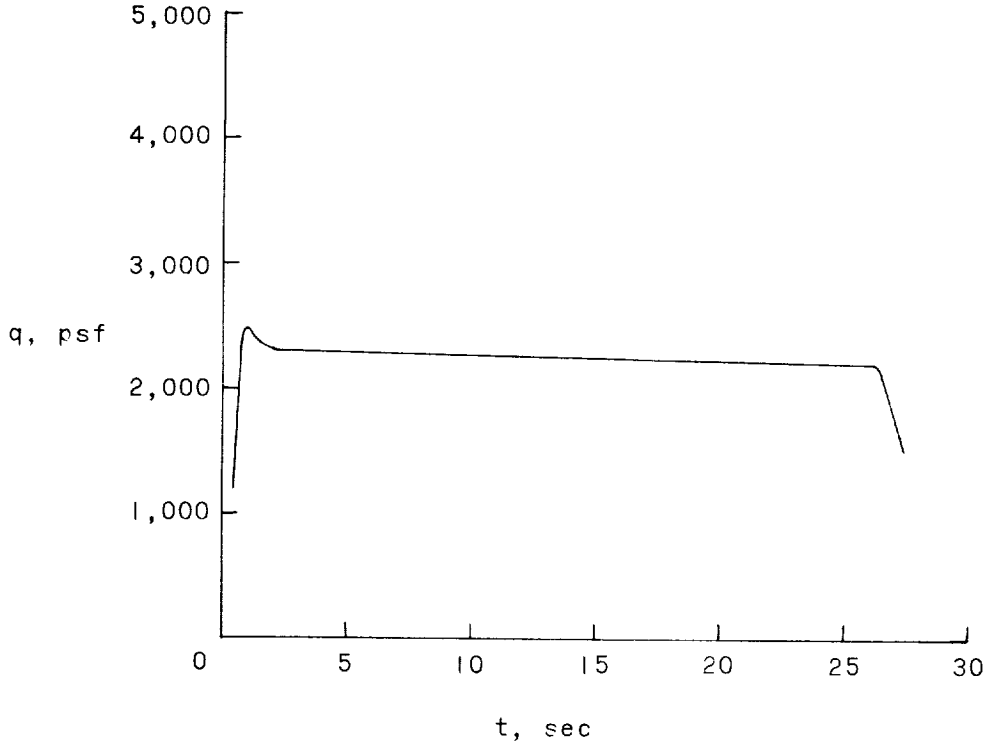

(b) Dynamic pressure.

Figure 18.- Pressure and temperature histories for the recoverable stabilizer. (Test 12.)

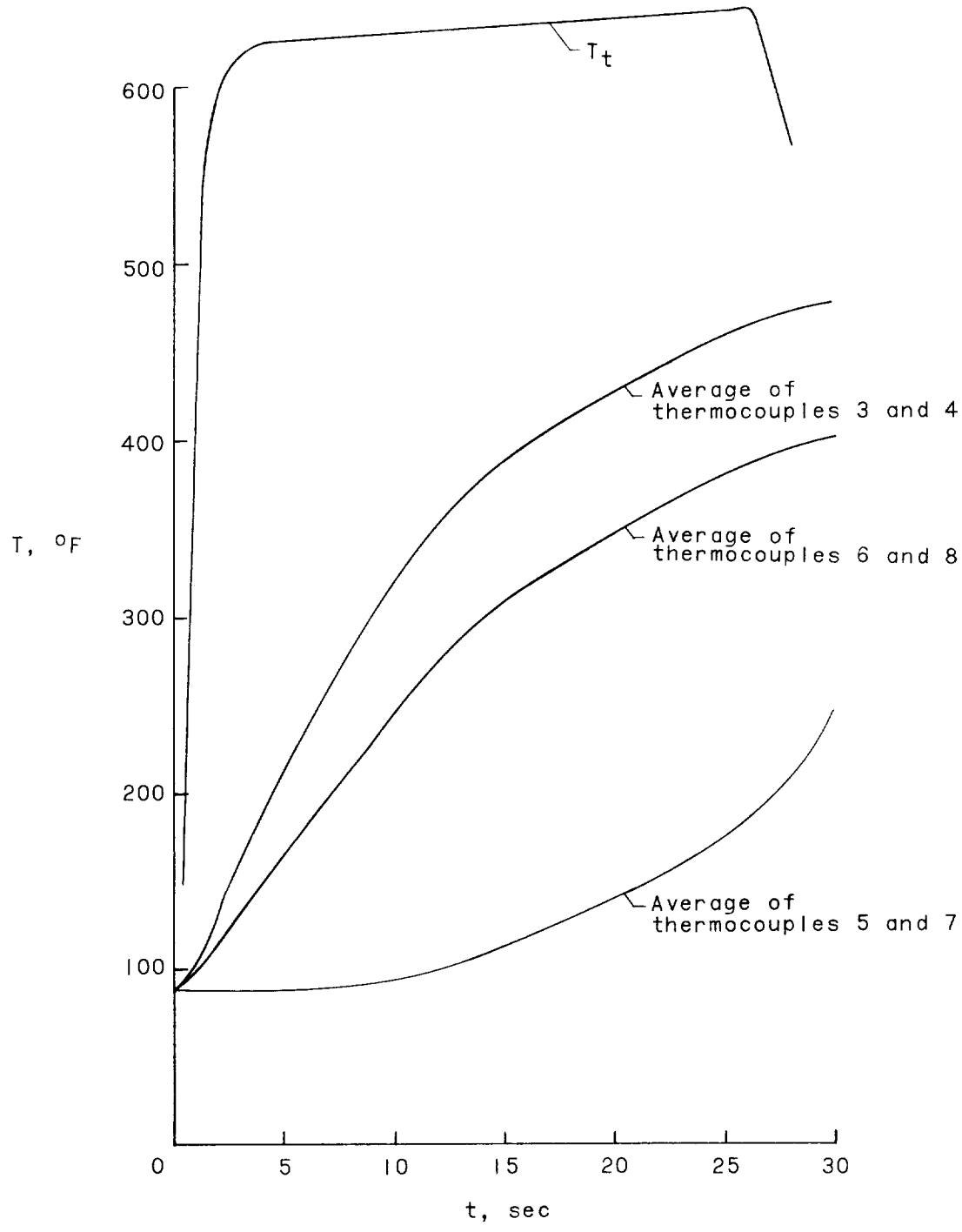

(c) Stagnation temperature and panel temperature.

Figure 18.- Concluded.

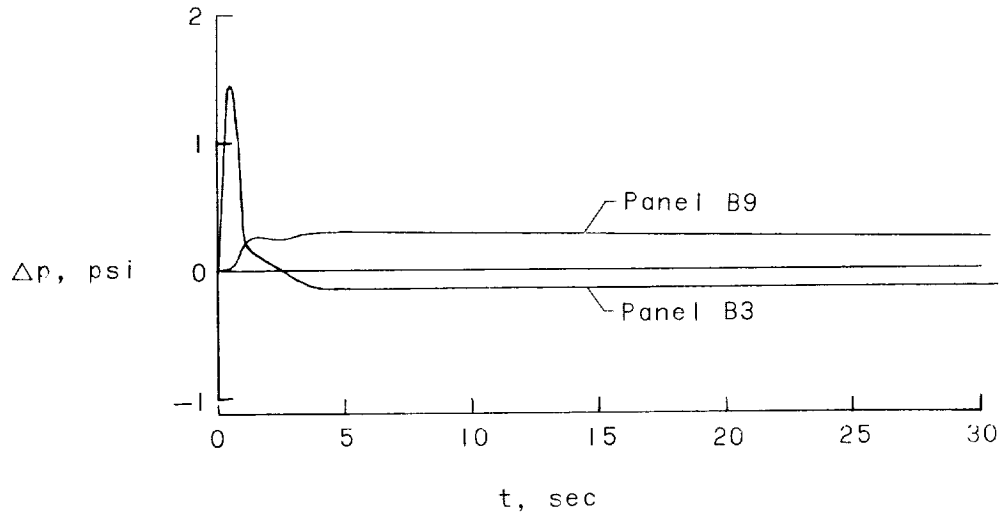

(a) Differential pressure.

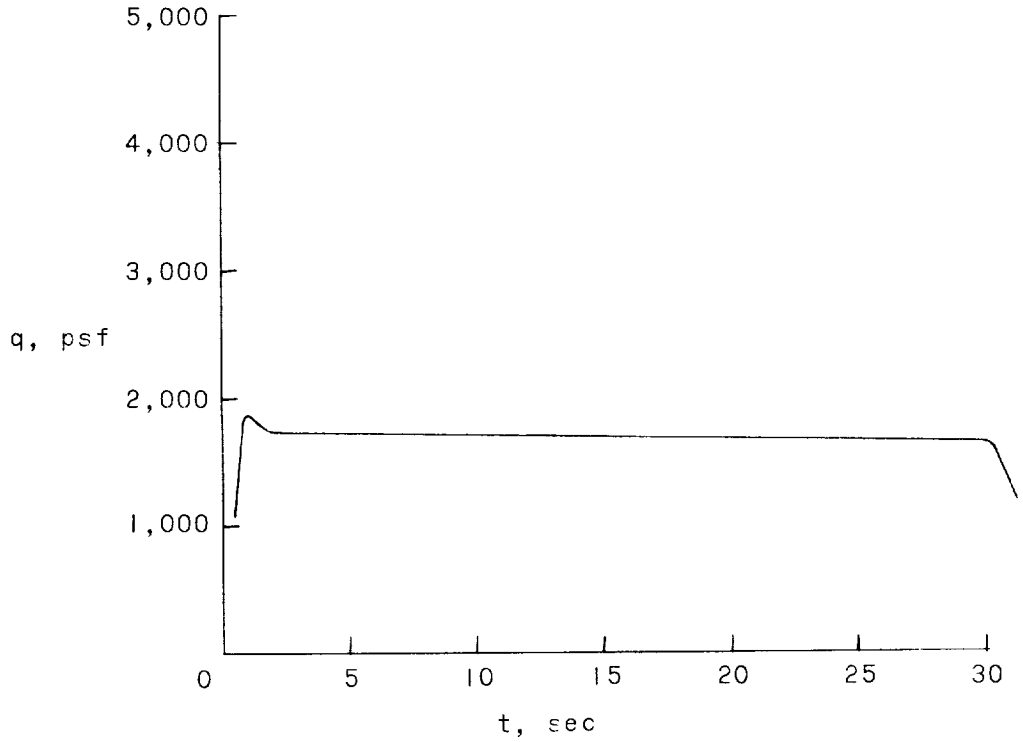

(b) Dynamic pressure.

Figure 19.- Temperature and pressure histories for the recoverable stabilizer. (Test 13.)

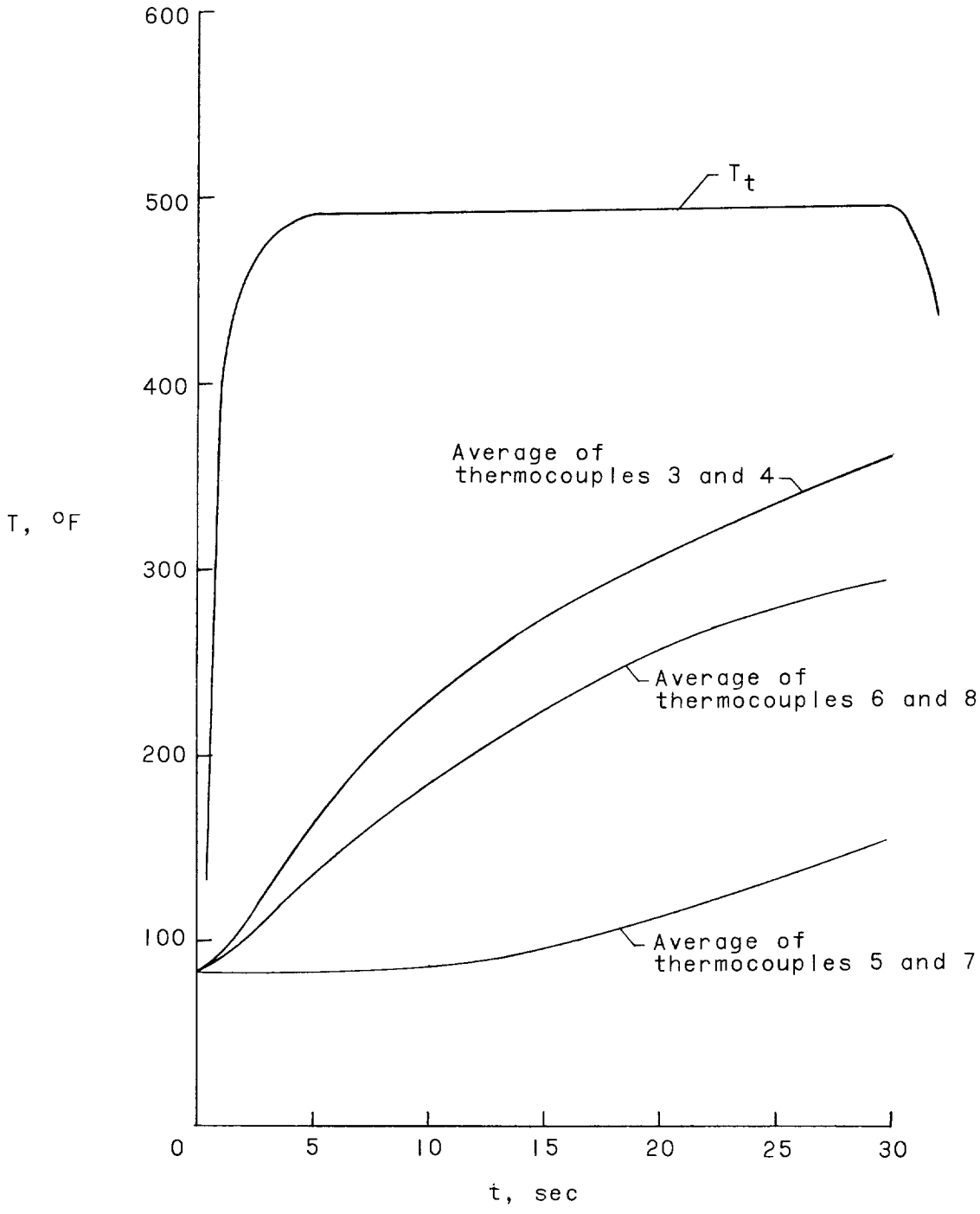

(c) Stagnation temperature and panel temperature.

Figure 19.- Concluded.

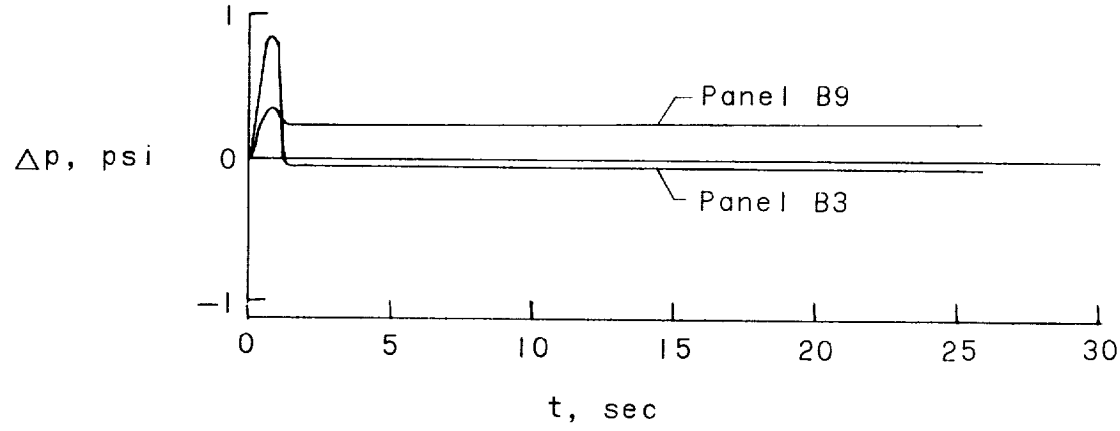

(a) Differential pressure.

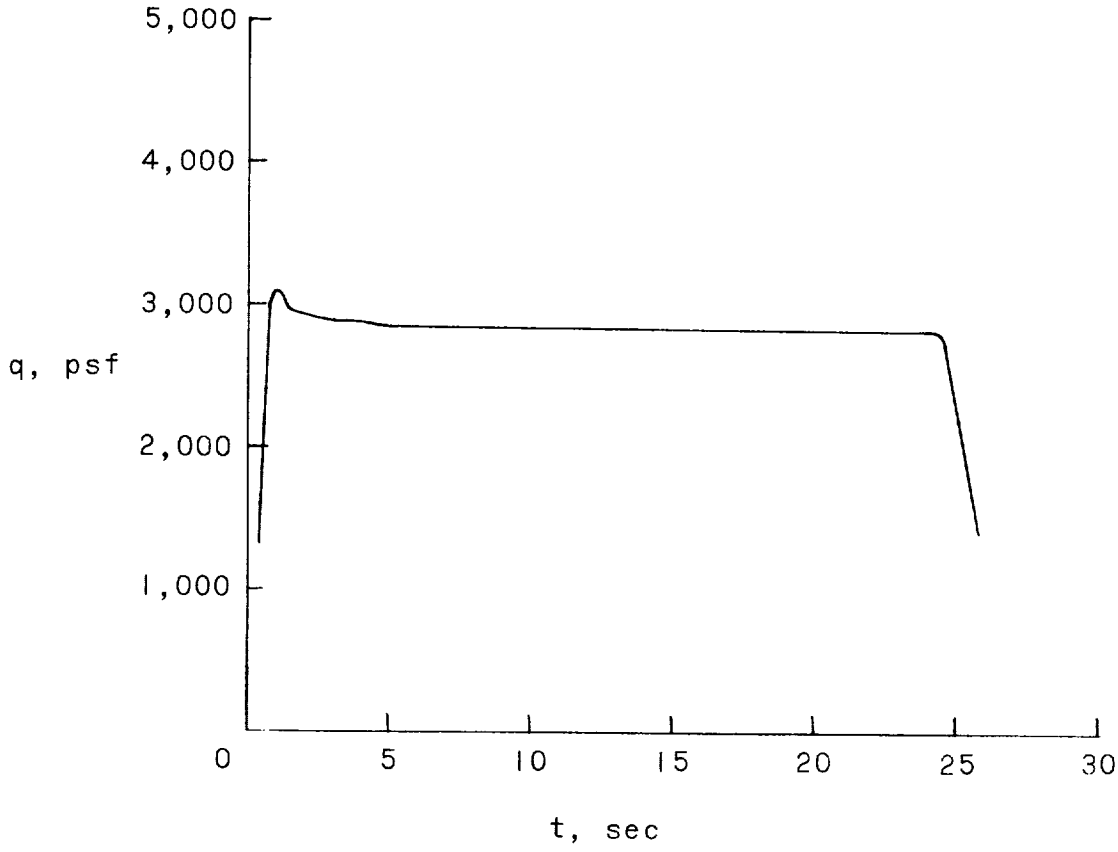

(b) Dynamic pressure.

Figure 20.- Temperature and pressure histories for the recoverable stabilizer. (Test 14.)

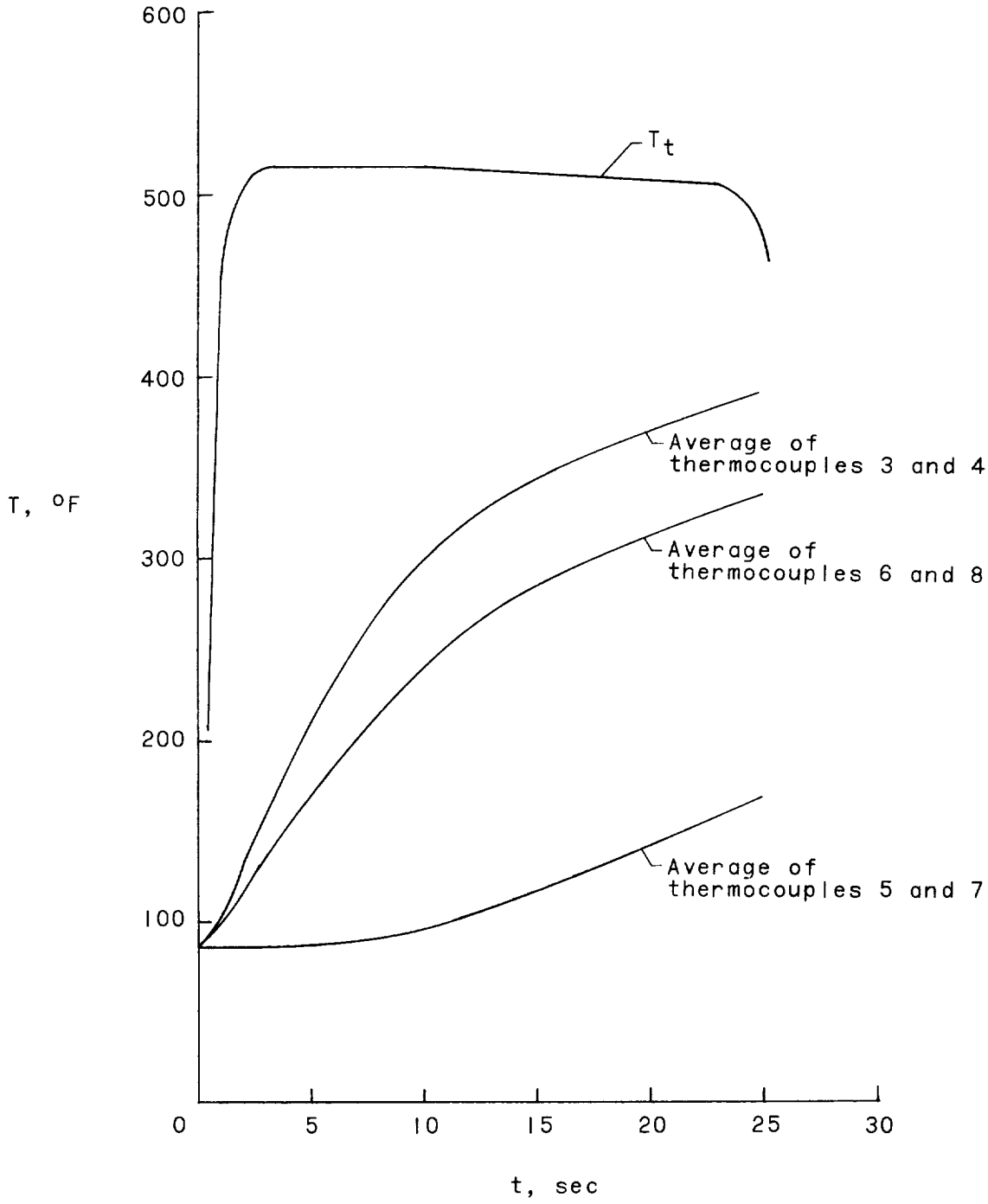

(c) Stagnation temperature and panel temperature.

Figure 20.- Concluded.

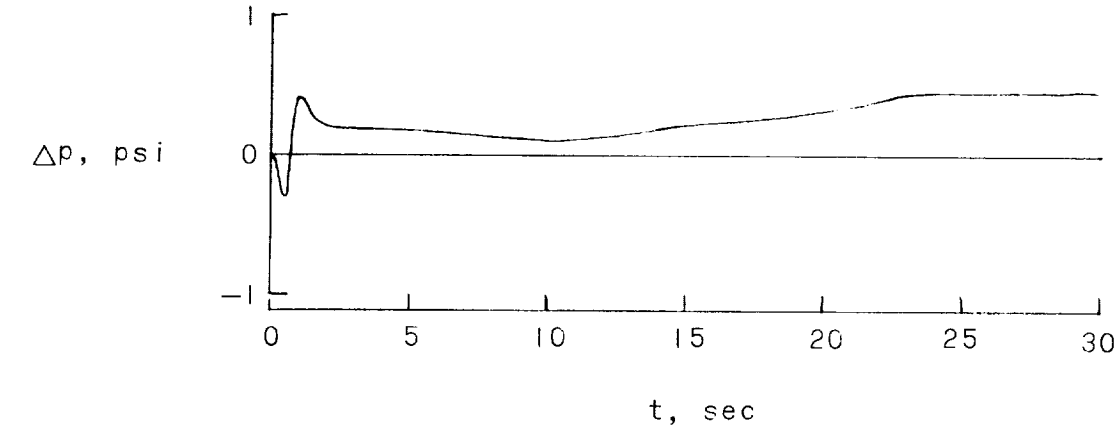

(a) Differential pressure (panel B9).

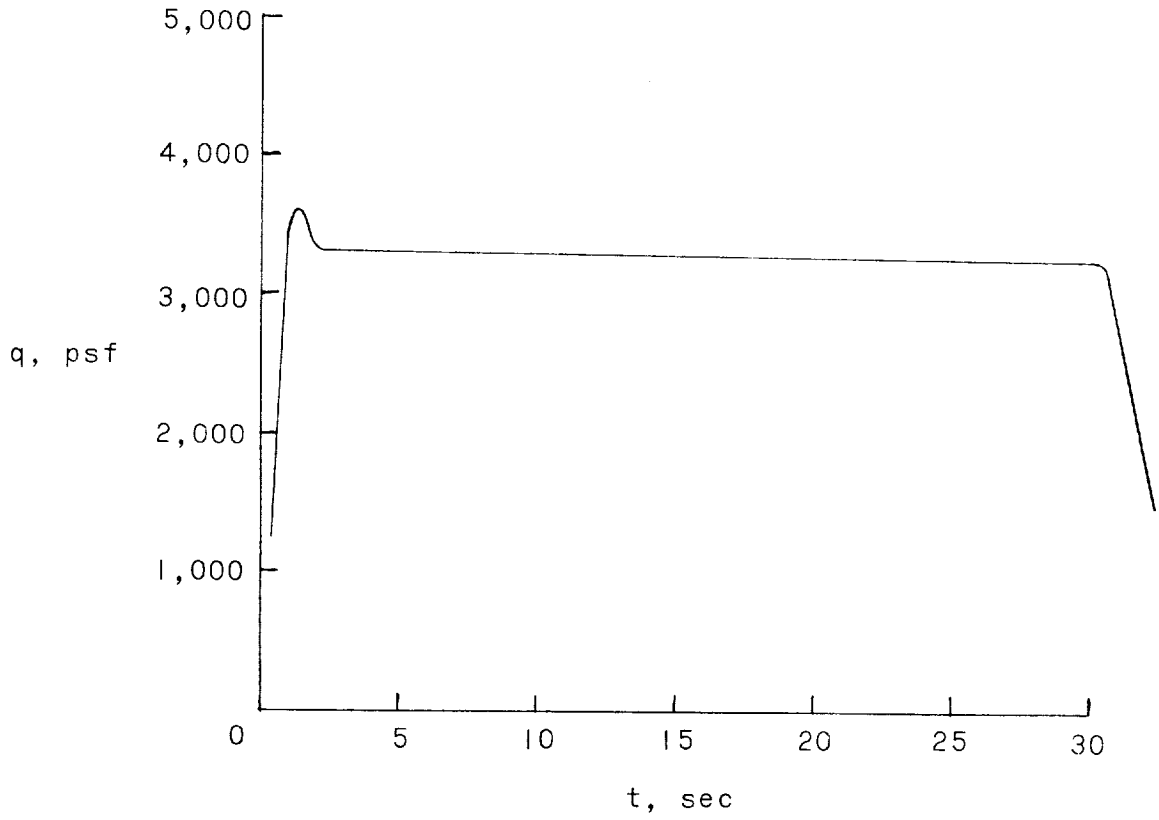

(b) Dynamic pressure.

Figure 21.- Pressure and temperature histories for the recoverable stabilizer. (Test 15.)

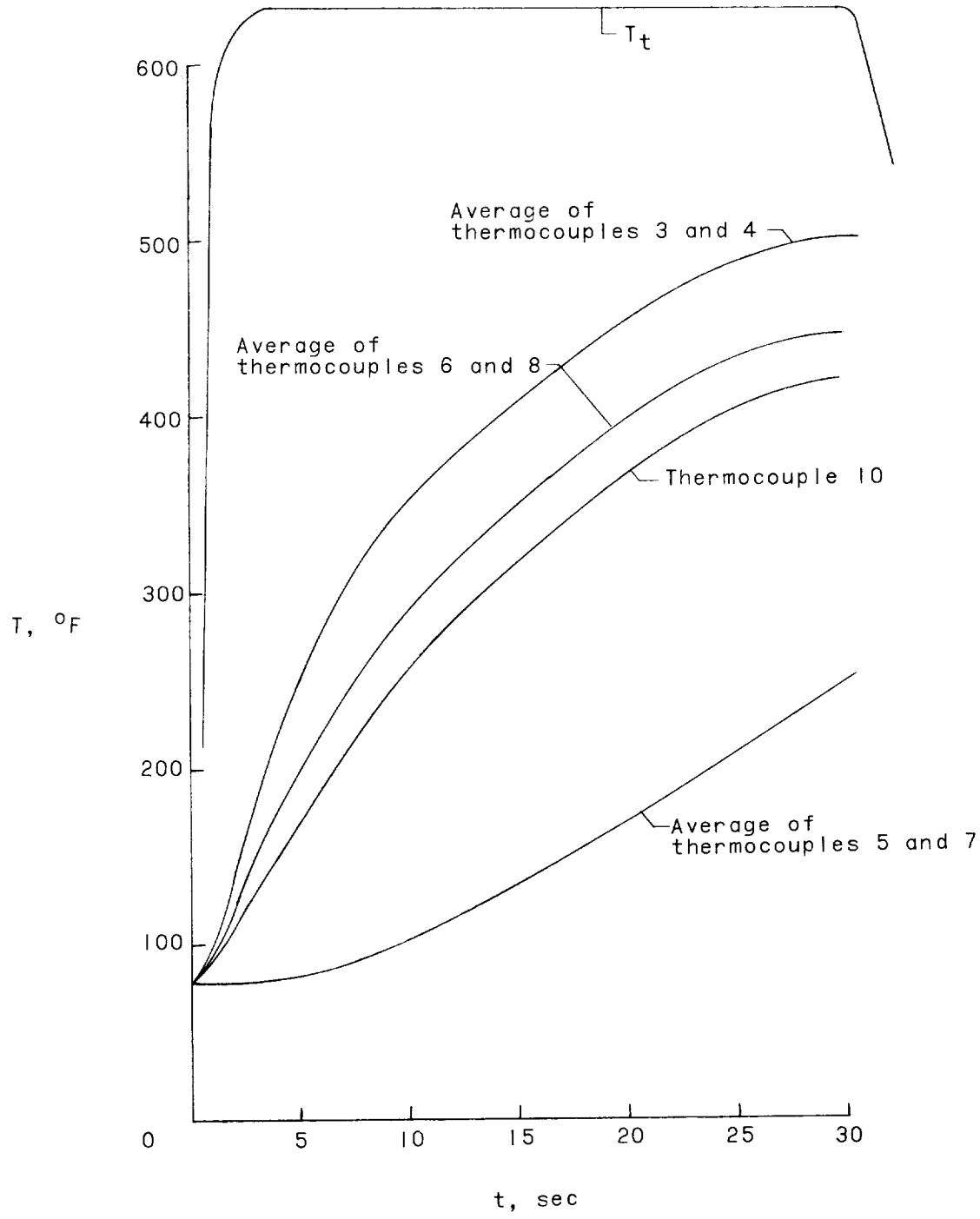

(c) Stagnation temperature and panel temperature.

Figure 21.- Concluded.

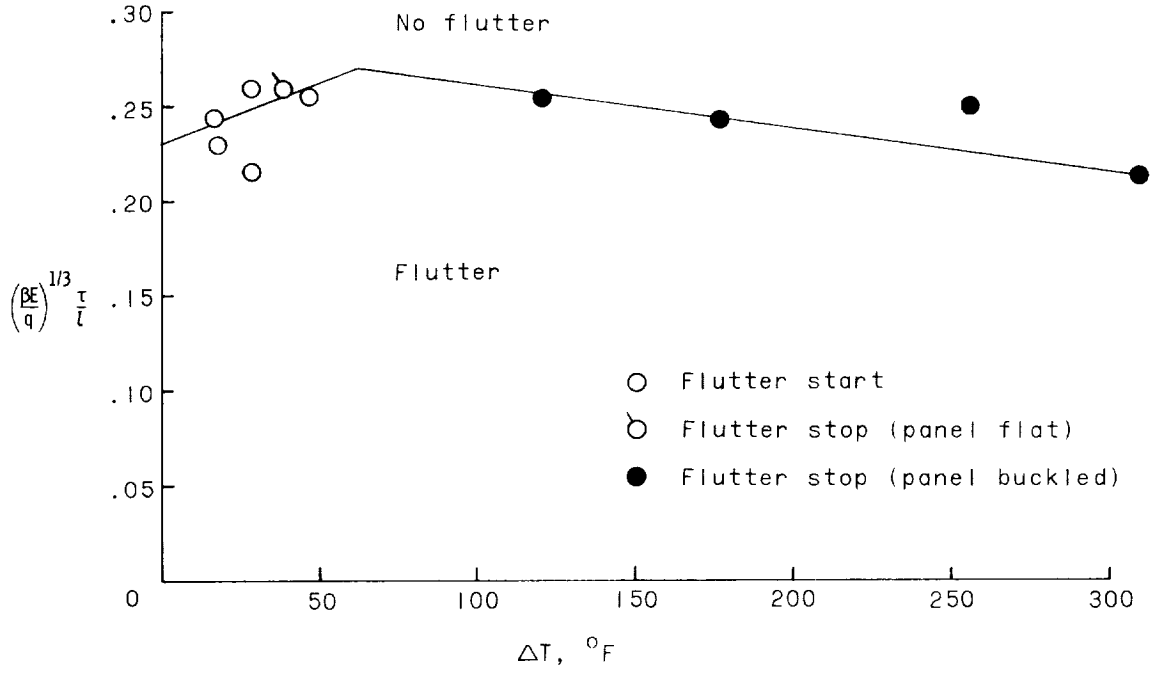

(a) Flutter boundary for length-width-ratio-4 panel.

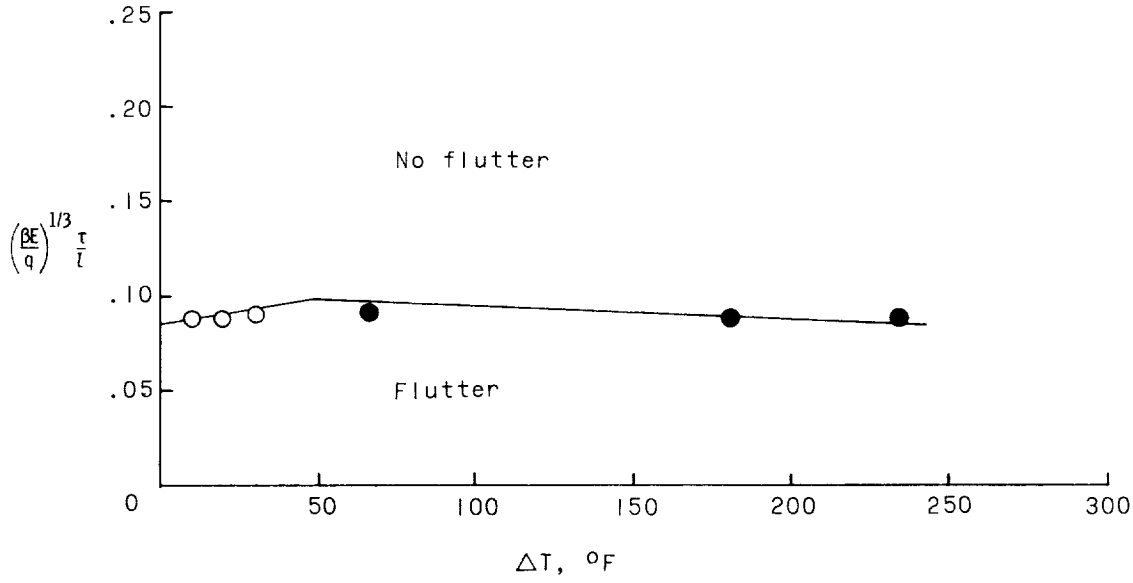

(b) Flutter boundary for length-width-ratio-10 panel.

Figure 22.- Flutter boundaries for unstiffened panels.

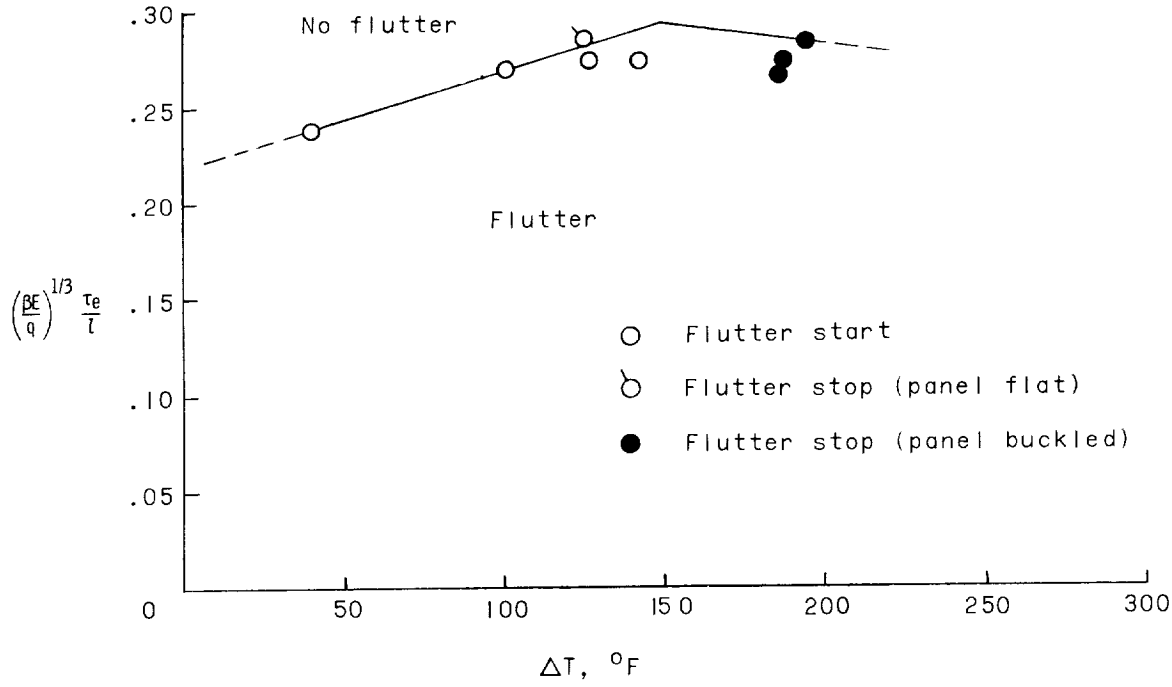

(a) Flutter boundary for length-width-ratio-1.5 panel.

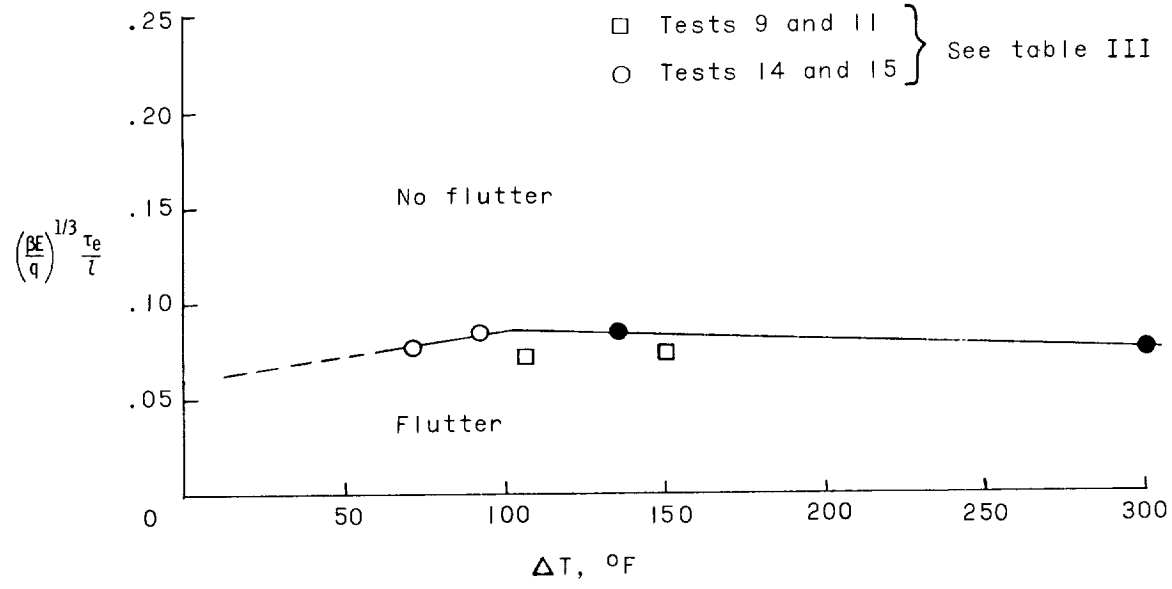

(b) Flutter boundary for length-width-ratio-10 panel.

Figure 23.- Flutter boundaries for corrugation-stiffened panels.

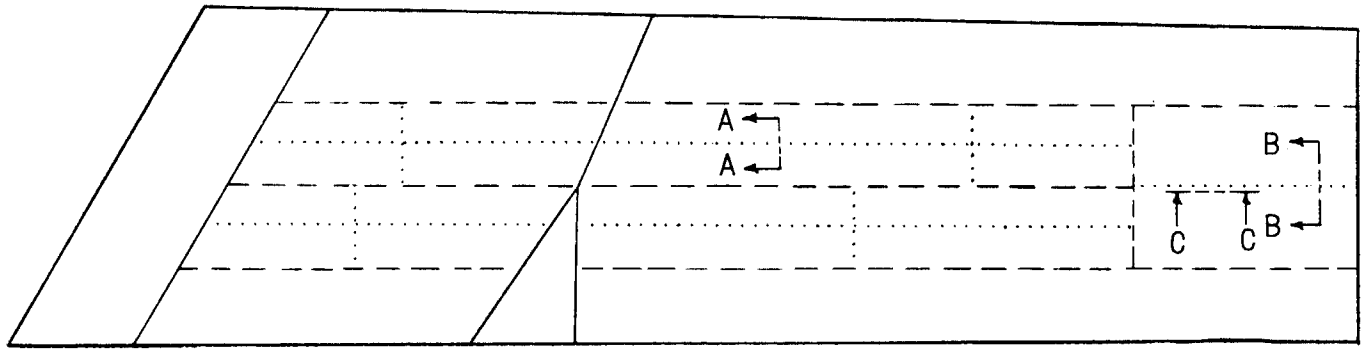

Left side

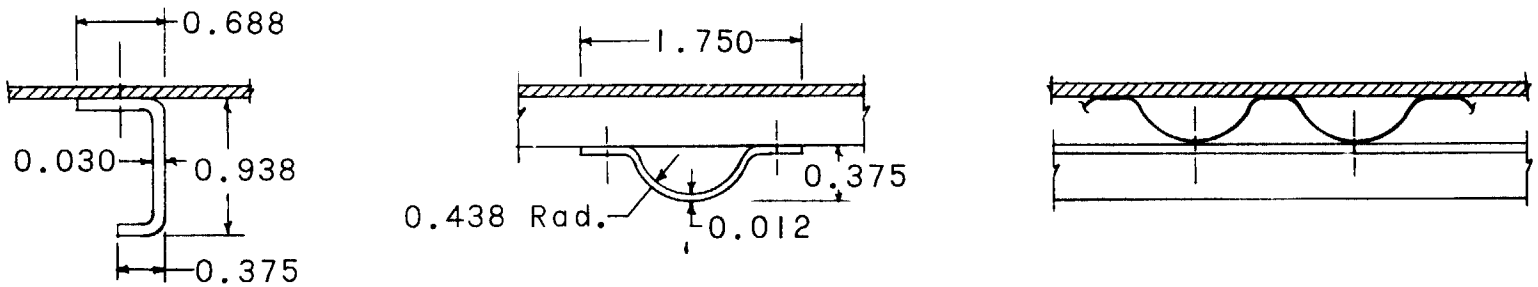

Section A—A Section B—B Section C—C

Figure 24.- Modifications to stabilizer panels. Added stiffeners indicated by dotted lines. (All dimensions are in inches.)

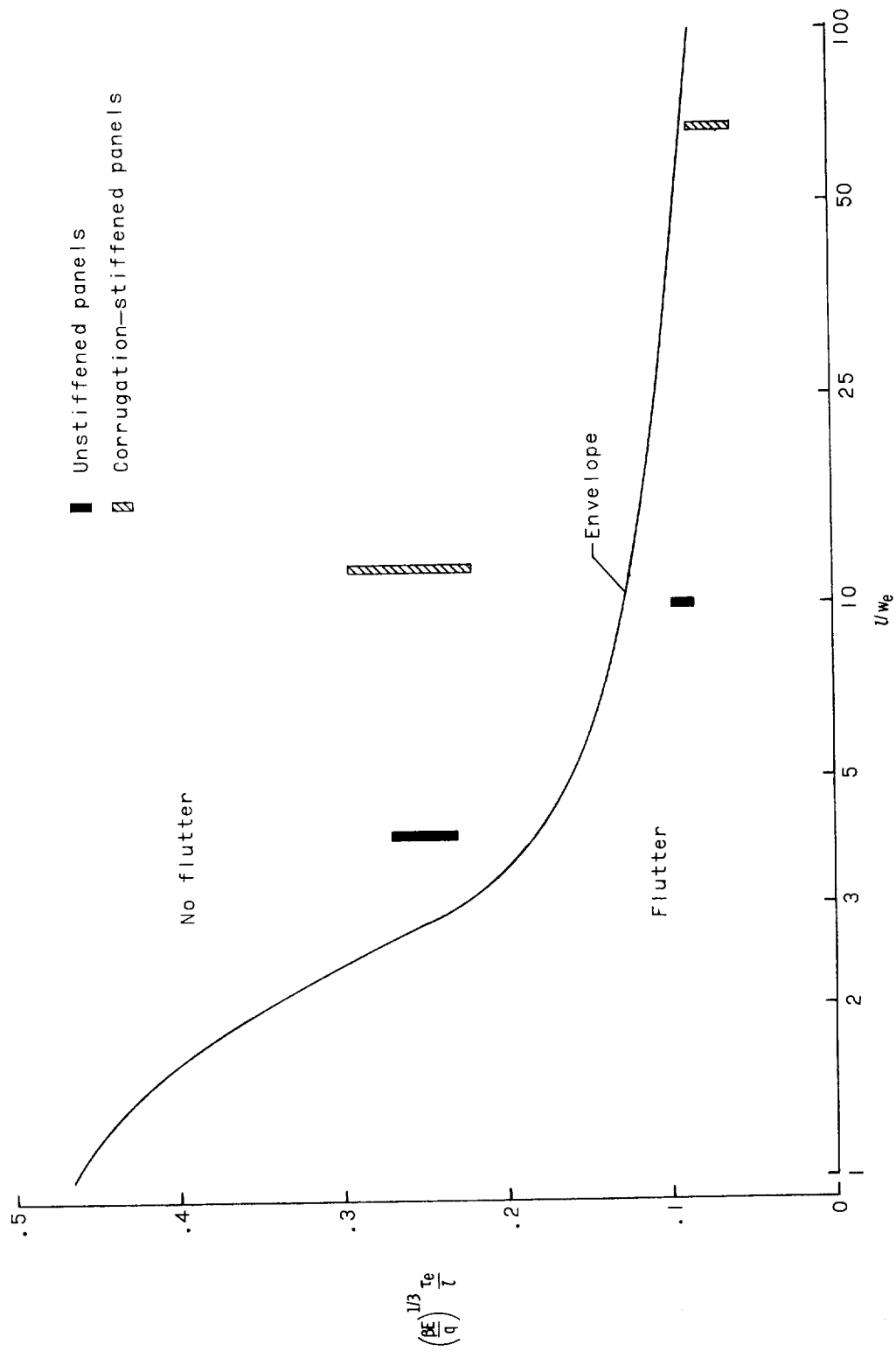

Figure 25.- Comparison of flutter results of present investigation with experimental envelope from reference 5.

NASA-Langley, 1962 L-1631